Diminished YAP1 affects mitochondrial dynamics in IDH1 mutant glioma

Shruti Patrick[1], Pruthvi Gowda[1], Kirti Lathoria[1], Vaishali Suri[2] and Ellora Sen[1]*

[1] National Brain Research Centre, Manesar-122052, India

[2] All India Institute of Medical Sciences, New Delhi-110029, India

***To whom correspondence should be addressed:**

National Brain Research Centre,

Nainwal Mode, NH-8, Manesar,

Haryana-122 052, India

Tele: 91-124-2845235

Fax: 91-124-2338910

Email: ellora@nbrc.ac.in;

Key words: Glioma, IDH1, YAP1, TFAM, TERT, Mitochondria

Summary Statement

Novel regulatory role of YAP1 in generation of mitochondrial ROS and TERT-mediated protective effect against oxidative stress could provide insights into the development of new anti-glioma strategies.

Abstract

Mutation in isocitrate dehydrogenase 1 (IDH1) gene, leading to the production of oncometabolite D-2-hydroxyglutarate (2-HG) from α-ketoglutarate, is associated with better prognosis in glioma. As Yes-associated protein 1 (YAP1) is an important regulator of tumor progression, its role in glioma expressing IDH1 R132H mutation was investigated. Diminished nuclear YAP1 in IDH1 mutant patient gliomas and cell lines was accompanied by decreased TFAM levels. Luciferase reporter assays and chromatin immunoprecipitation indicated the functionality of TEAD2 site on TFAM promoter in mediating its YAP1-dependent expression. YAP1-dependent mitochondrial fragmentation and ROS generation was accompanied by decreased TERT levels and increased mitochondrial TERT localization in IDH1 R132H cells. Treatment with Bosutinib that prevents extranuclear TERT shuttle, further elevated ROS in IDH1 R132H cells and triggered apoptosis. Importantly, Bosutinib elevated ROS levels and induced apoptosis in IDH1 WT cells upon concurrent depletion of YAP1. These findings highlight the involvement of YAP1 in coupling mitochondrial dysfunction with TERT mitochondrial shuttle to constitute an essential non-canonical function of YAP1 in regulating redox homeostasis.

Introduction

Somatic mutations in the isocitrate dehydrogenase 1 (IDH1) gene are common in lower grade diffuse gliomas and secondary glioblastomas, with point mutation IDH1 R132H being the most prevalent (Parsons et al., 2008). IDH1 R132H is a dominant gain-of-function mutation which causes a shift in substrate specificity where IDH1 enzyme catabolizes α-ketoglutarate into oncometabolite D-2-hydroxyglutarate (2-HG) in an NADPH-dependent reaction (Bleeker et al., 2010). As a consequence, significantly higher levels of 2-HG are found in IDH1 R132H gliomas as compared to those without the mutation (Dang et al., 2009). The mutation affects various key signaling pathways (Gowda et al., 2018), including downregulation of Yes-associated protein 1 (YAP1) and Notch signaling (Wei et al., 2018).

Transcriptional coactivator YAP1 is the major downstream effector of the Hippo signaling pathway which is involved in tissue growth, repair, regeneration, cell proliferation and apoptosis (Ouyang et al., 2020). The core components of Hippo pathway Mammalian STE20-like protein kinases (MST1/2) and Large Tumor Suppressor Kinases (LATS1/2) are involved in

phosphorylation, cytoplasmic retention, and ultimately proteasomal degradation of YAP1 (Zhao et al., 2010). YAP1, overexpressed in several solid tumors including glioma (Orr et al., 2011), is not only linked to the molecular subtype of gliomas but is also associated with patient prognosis (Guichet et al., 2018). In addition, YAP1 and its downstream signaling pathway Notch is associated with reduced growth of IDH1 mutant astroglial cells (Wei et al., 2018). YAP1 is translocated into the nucleus where it associates with members of the TEA domain containing transcription factors (TEADs). YAP1/TEAD complexes regulate genes required for growth and oncogenic transformation (Zhao et al., 2008).

YAP1 is known to regulate mitochondrial structure, function and biogenesis (Mammoto et al., 2018). Mitochondria in cancers have an altered bioenergetic state, and dysregulated mitochondrial metabolism leads to increase in mitochondrial reactive oxygen species (mtROS) levels (Wallace, 2012). Mitochondrial transcription factor A (TFAM) - a nuclear-encoded protein essential for packaging, replication, and transcription of mitochondrial DNA (mtDNA) is responsible for its maintenance and biogenesis (Picca and Lezza, 2015). TFAM is upregulated in a number of cancers including gliomas (Hu et al., 2020), and depletion of TFAM is associated with reduced mtDNA copy number, elevated ROS, as well as sensitivity to chemotherapeutic drugs (Mei et al., 2015). IDH1 mutants, characterized by consumption of NADPH to synthesize 2-HG, have decreased levels of reducing power, thereby making them more susceptible to change in cellular redox status (Khurshed et al., 2018). IDH1 mutation is also associated with altered mitochondrial function (Li et al., 2015).

mtDNA is highly susceptible to ROS-mediated damage and is repaired and protected by a number of mechanisms. One such mechanism involves the reversible nuclear exclusion and mitochondrial localization of telomerase reverse transcriptase (TERT) (Ahmed et al., 2008), the enzymatic subunit of the telomerase complex responsible for maintenance of telomeres. TERT is regulated by a number of signaling pathways, one of which is the Hippo/YAP1 pathway (Zhang et al., 2020b), and telomerase activity is associated with proliferation potential of several malignancies including gliomas (Lee et al., 2017). Telomere dysfunction represses mitochondrial biogenesis, reduces mitochondrial DNA content, and decreases mitochondrial mass and energy production (Sahin et al., 2011). Mitochondrial integrity is critical for cell survival, and TERT binds mtDNA to protect against ROS (Ahmed et al., 2008, Haendeler et al., 2009). Defects in

telomeres induced by dysregulated mitochondria are crucial in regulating telomere-mitochondria crosstalk in response to mitochondrial ROS levels (Qian et al., 2019). IDH1 mutation-induced elevated ROS is associated with increased chemosensitivity in glioma cells (Shi et al., 2015). Besides, IDH1 mutational status (Garrett et al., 2018) and YAP1 expression have been suggested as a prognostic biomarker and potential therapeutic target in glioma (Guichet et al., 2018). Since both mitochondrial and telomere functions are critical for cancer (Blasco, 2005, Giampazolias and Tait, 2016); and as YAP1 is known to regulate both mitochondrial function and TERT levels; this study was undertaken to evaluate the functional crosstalk between YAP1, TERT and mitochondrial dynamics in gliomas harboring IDH1 mutation.

Results

Diminished YAP1 expression in IDH1 R132H is C-Jun dependent

As demonstrated previously (Wei et al., 2018), the Cancer Genome Atlas (TCGA) data analysis shows diminished YAP1 levels in gliomas harboring IDH1 R132H mutation as compared to IDH1 WT tumors (Fig. S1A). A decrease in YAP1 mRNA (Fig. 1A) and protein levels (Fig. 1B, S1B) were found in IDH1 R132H cells as compared to IDH1 WT cells. A similar decrease in YAP1 level was observed in T98G cells transiently transfected with IDH1 R132H (Fig. S1C). IDH1 mutant cancers are hallmarked by aberrant accumulation of the metabolite 2-HG which mediates many of the phenotypes observed in these cancers. Decreased YAP1 was also observed in LN18 cells treated with 2-HG (Fig. 1C, S1D). Further, immunohistochemical staining of patient-derived tumor tissue sections showed decreased levels of YAP1 in IDH1 mutant gliomas (Fig. 1D). A similar decrease in YAP1 levels in IDH1 R123H mutant astroglial cells has been reported (Wei et al., 2018).

YAP1 levels are controlled by the Hippo pathway (Dong et al., 2007), and YAP1 expression is also directly regulated by Wnt/β-catenin signaling (Konsavage et al., 2012). However, since neither Hippo pathway nor Wnt signaling are responsible for reduced YAP1 levels in IDH1 R132H cells (Wei et al., 2018), we looked into other potential candidate molecules which could function upstream in regulating YAP1. It has been shown that YAP1 expression is dependent on transcription factor C-Jun (Zhang et al., 2020a). TCGA data showed diminished JUN levels in gliomas harboring IDH1 R132H as compared to IDH1 WT gliomas (Fig. 1E). A decrease in C-Jun, as well as transcriptionally active phosphorylated C-Jun, was seen in IDH1

R132H cells (Fig. 1F, Fig. S1E) and 2-HG treated LN18 cells (Fig. 1G). On further investigating the status of C-Jun N-terminal kinase (JNK) - the upstream activator of C-Jun, and its active phosphorylated form, no difference between their levels in IDH1 WT and R132H cells was observed (Fig 1H, Fig. S1F). To confirm the role of C-Jun in regulating YAP1 expression, we treated IDH1 WT cells exhibiting heightened C-Jun levels with JNK inhibitor SP600125 which inhibits the phosphorylation and activation of C-Jun. Treatment with SP600125 reduced YAP1 levels suggesting C-Jun-dependent regulation of YAP1 (Fig. 1I, Fig. S1G).

Diminished YAP1 is accompanied by reduced nuclear TEAD2 levels in IDH1 R132H

Since YAP1 is a transcriptional coactivator that is functional within the nucleus, nuclear YAP1 protein levels in the cells were investigated. A decrease in nuclear YAP1 levels was observed in IDH1 R132H cells (Fig. 2A, Fig. S2A), as well as in LN18 cells treated with 2-HG (Fig. 2B, Fig. S2B). Immunohistochemical staining of tissue sections derived from patients showed higher levels of nuclear YAP1 in IDH1 WT gliomas as compared to IDH1 mutants (Fig. 1D, Fig. 2C).
TEAD family transcription factors are crucial for YAP1-mediated gene transcription (Zhao et al., 2008). In case of IDH1 R132H cells, the decrease in nuclear YAP1 levels was accompanied by reduced nuclear levels of TEAD2 (Fig. 2D, Fig. S2C). LN18 cells treated with 2-HG also showed diminished nuclear TEAD2 levels (Fig. 2E, Fig. S2D). Co-immunoprecipitation showed reduced levels of YAP1/TEAD2 complex in IDH1 R132H as compared to IDH1 WT (Fig. S2E).
Luciferase reporter assays in IDH1 WT and IDH1 R132H cells transfected with 8xGTIIC construct containing YAP1 responsive synthetic promoter showed that TEAD-mediated YAP1 activity was diminished in IDH1 R132H cells (Fig. 2F). Analysis of the levels of known TEAD target genes using data from TCGA further indicated decrease in YAP1/TEAD transcriptional activity in IDH1 R132H gliomas (Fig. S2F-P).

YAP1/TEAD2 is involved in regulating TFAM expression

YAP1 regulates mitochondrial structure and function (Nagaraj et al., 2012) as well as mitochondrial biogenesis (Mammoto et al., 2018). Since synthesis of mtDNA is essential for mitochondrial biogenesis, we looked into the mtDNA content of IDH1 R132H cells with diminished YAP1 levels. A reduction in mtDNA copy number was observed in IDH1 R132H cells as compared to IDH1 WT cells (Fig. 3A). As TFAM regulates mtDNA copy number (Campbell et

al., 2012, Ekstrand et al., 2004), and is necessary for mitochondrial biogenesis and function, its status was investigated in IDH1 R132H cells with diminished YAP1 levels. Decrease in TFAM protein level was observed in IDH1 R132H cells as compared to IDH1 WT cells, in LN18 cells treated with 2-HG (Fig. 3B, Fig. S3A) as well as in T98G cells transiently transfected with IDH1 R132H (Fig. S3B). Immunohistochemical staining of patient-derived tumor tissue sections showed decreased levels of TFAM in IDH1 mutant gliomas as compared to WT (Fig. 3C).

The decrease in TFAM was YAP1-dependent as siRNA-mediated knockdown of YAP1 in IDH1 WT cells diminished TFAM levels while overexpression of YAP1 in IDH1 R132H cells led to an increase (Fig. 3D, Fig. S3C). As TEAD2 binding site was predicted on the TFAM promoter (position: 625 to 635) using ALGGEN PROMO version 3.0.2 which uses version 8.3 of TRANSFAC (Farre et al., 2003) (Fig. 3E), ChIP was performed to determine whether TEAD2 binding to this site regulates TFAM expression. A higher enrichment of TEAD2 at its predicted binding site on TFAM promoter was observed in IDH1 WT as compared to IDH1 R132H cells, along with a higher enrichment of RNA pol II (Fig. 3E); suggesting the regulation of TFAM expression by YAP1/TEAD2 complex. GAPDH promoter was used as negative control for ChIP.

The dependence of TFAM on YAP1/TEAD2 complex was further confirmed by luciferase reporter assays using constructs containing either the wild type TFAM promoter (TFAM WT luciferase) or TFAM promoter with mutation in the predicted TEAD2 binding site (TFAM Δ luciferase) (Fig. 3F). A decrease in TFAM WT luciferase activity was observed in IDH1 R132H cells as compared to IDH1 WT cells transfected with the same construct (Fig. 3G). In addition, TFAM Δ luciferase showed reduced activity as compared to TFAM WT luciferase in IDH1 WT cells (Fig. 3H). The role of YAP1 in the expression of TFAM was further validated using S94A mutant YAP1 which disrupts its binding to the TEAD transcription factors. While overexpression of wild type YAP1 in IDH1 R132H cells brought about an increase in TFAM protein levels, there was no such increase on overexpressing YAP1-S94A (Fig. 3I, Fig. S3D). These experiments with TFAM luciferase reporters (TFAM WT or TFAM Δ), together with overexpression of wild type and S94A mutant YAP1, demonstrated that YAP1/TEAD2 interaction is indeed involved in regulating TFAM expression.

Increased mitochondrial fragmentation in IDH1 R132H glioma

The morphology and distribution of the mitochondrial network are maintained through the dynamic balance between fission and fusion, which involves the essential role of mitofusins (Ishihara et al., 2004) and Dynamin-related protein 1 (DRP1) (Imoto et al., 1998) among others. Investigation of mitochondrial morphology in the cells using MitoTracker staining showed that mitochondria in IDH1 R132H cells had a more fragmented appearance, while IDH1 WT cells had more fused and branched mitochondria (Fig. 4A). Mitofusin 1 (MFN1) is essential for mitochondrial fusion and maintenance of mitochondrial morphology. Analysis of TCGA data showed lower levels of MFN1 in IDH1 R132H gliomas as compared to wild type (Fig. 4B). Diminished levels of MFN1 were observed in IDH1 R132H cells and in 2-HG-treated LN18 cells (Fig. 4C, Fig. S4A). Similar decrease in MFN1 levels were observed in T98G cells transiently expressing IDH1 R132H (Fig. S4B). MFN1 expression was found to be YAP1-dependent, since knockdown of YAP1 in IDH1 WT cells decreased MFN1 levels (Fig. 4D, Fig. S4C), while YAP1 overexpression in IDH1 R132H cells increased MFN1 (Fig 4D, Fig. S4D). In addition to a decrease in MFN1, TCGA data also revealed an increase in DRP1 levels in IDH1 R132H gliomas (Fig. S4E). While the total DRP1 protein levels were found to be lower in IDH1 R132H cells as compared to IDH1 WT (Fig. S4F), immunoblot analysis of mitochondrial protein fractions showed an increase in DRP1 recruitment to the mitochondria in IDH1 R132H cells (Fig. S4G).

Diminished YAP1 increases mitochondrial fragmentation and ROS accumulation in IDH1 R132H

Fragmentation of mitochondria was also found to be dependent on YAP1; siRNA-mediated knockdown of YAP1 in IDH1 WT cells led to increased mitochondrial fragmentation (Fig. 5A), while overexpression of YAP1 in IDH1 R132H cells led to a decrease (Fig. 5B).

As TFAM depletion as well as mitochondrial fission are associated with elevated mitochondrial ROS (Woo et al., 2012), the status of ROS in IDH1 R132H cells with diminished TFAM and MFN1 levels was determined. MitoSOX Red staining revealed higher levels of mitochondrial ROS in IDH1 R132H cells as compared to IDH1 WT cells (Fig. 5C), as well as in LN18 cells treated with 2-HG (Fig. 5D). This increase was found to be YAP1-dependent, since siRNA-mediated knockdown of YAP1 led to an elevation in mitochondrial ROS in IDH1 WT cells (Fig.

5E), while overexpression of YAP1 in IDH1 R132H cells resulted in a reduction in mitochondrial ROS (Fig. 5F).

Increased mitochondrial ROS is concomitant with altered localization and reduced expression of TERT

Given the protective function of TERT in mitochondria under conditions of oxidative stress (Ahmed et al., 2008), we investigated the subcellular localization of TERT in IDH1 R132H cells and in 2-HG-treated LN18 cells exhibiting elevated mitochondrial ROS levels. Immunoblot analysis of mitochondrial and nuclear protein fractions showed an increase in mitochondrial localization of TERT in case of IDH1 R132H cells as compared to IDH1 WT cells (Fig. 6A). The extranuclear shuttle of TERT upon 2-HG treatment, was reduced on overexpression of YAP1 in 2-HG-treated cells (Fig. 6B). This reduction in mitochondrial TERT localization was concomitant with diminished ROS levels observed upon YAP1 overexpression (Fig. 5F). The results suggest the involvement of mitochondrial ROS in the translocation of TERT into the mitochondria.
As YAP1 hyperactivation promotes telomerase activity, increases telomere length and expression of TERT (Zhang et al., 2020b), the status of TERT in IDH1 mutants exhibiting diminished YAP1 was investigated. TCGA data revealed diminished TERT levels in IDH1 R132H gliomas as compared to the wild type (Fig. 6C). A decrease in TERT mRNA (Fig S5A) and protein (Fig. 6D, Fig. S5B) levels was observed in IDH1 R132H cells. Reduced TERT levels were also found in 2-HG-treated LN18 cells (Fig. 6D, Fig. S5B), and in T98G cells transiently expressing IDH1 R132H (Fig. S5C). Diminished TERT expression in IDH1 R132H cells was accompanied by reduced telomerase activity (Fig. S5D) and decreased telomere length (Fig. S5E). As decrease in nuclear YAP1 was concomitant with diminished TERT expression, the role of YAP1 in the expression of TERT was investigated. While siRNA-mediated knockdown of YAP1 in IDH1 WT cells diminished TERT expression (Fig. 6E, Fig. S5F) and telomerase activity (Fig. S5F), overexpression of YAP1 in IDH1 R132H cells resulted in increased TERT expression (Fig. 6E, Fig. S5G) and telomerase activity (Fig. S5G). In order to corroborate the involvement of YAP1 in regulating the expression of TERT, YAP1-S94A mutant was employed. Overexpression of wild-type YAP1 in IDH1 R132H cells led to an increase in TERT levels, but no such increase was seen on overexpressing YAP1-S94A (Fig. 6F, Fig. S5H). The results suggest that YAP1 regulates TERT expression and this regulation is TEAD-dependent.

YAP1-mediated mitochondrial translocation of TERT affects ROS generation

Mitochondrial localization of TERT protects cells from oxidative stress-induced apoptosis (Miwa et al., 2016). As nuclear exclusion and mitochondrial targeting of TERT are employed by cells under conditions of oxidative stress, we next investigated whether inhibition of TERT translocation to mitochondria affects ROS generation to subsequently alter the susceptibility to oxidative stress-mediated death. We treated IDH1 WT and IDH1 R132H cells with Src kinase inhibitor, Bosutinib, which blocks TERT nuclear exclusion and mitochondrial localization (Miwa et al., 2016). While Bosutinib treatment led to a moderate increase in mitochondrial ROS levels in IDH1 WT cells, it caused a more pronounced elevation of mitochondrial ROS in IDH1 R132H cells (Fig. 7A). Elevation in mitochondrial ROS was also observed upon Bosutinib treatment in LN18 cells pretreated with 2-HG (Fig. 7B). While Bosutinib treatment alone was sufficient to considerably raise mitochondrial ROS in IDH1 R132H cells (Fig. 7A), siRNA-mediated knockdown of YAP1 was required in conjunction with Bosutinib to bring about a similar increase in ROS levels in IDH1 WT cells (Fig. 7C). Overexpressing YAP1 in IDH1 R132H cells prevented Bosutinib treatment-induced increase in mitochondrial ROS levels, thus highlighting the involvement of YAP1 in responsiveness to Bosutinib treatment (Fig. 7D). Though cells export TERT to mitochondria under conditions of oxidative stress, the decreased TERT levels in IDH1 R132H cells dampens their ability to tolerate heightened ROS generation. This renders these cells more susceptible to blockers of TERT nuclear export. This effect of inhibiting mitochondrial targeting of TERT is evident in IDH1 WT cells when overall TERT levels are lowered upon YAP1 knockdown.

Inhibition of extranuclear shuttling of TERT into mitochondria affects apoptotic mediators

We next investigated whether extranuclear shuttling of TERT in IDH1 R132H affects survival responses under conditions of elevated oxidative stress. Heightened ROS generation upon inhibition of mitochondrial TERT shuttle by Bosutinib was accompanied by increased levels of pro-apoptotic markers, cleaved Caspase 3 (Fig. 7E), BAX vs BCL2 ratio (Fig. S6A), and cleaved PARP (Fig. S6B). TUNEL assay indicated apoptotic cell death in Bosutinib-treated IDH1 R132H cells (Fig. 7F, Fig. S6C). The sensitivity of IDH1 R132H-expressing cells to ROS induction and cell death on Bosutinib treatment was further confirmed upon treatment with ROS scavenger N-Acetyl-L-cysteine (NAC). Co-treatment with ROS scavenger NAC abolished Bosutinib-induced

death in IDH1 R132H cells (Fig. 7G). In case of IDH1 WT cells, Bosutinib treatment or YAP1 knockdown alone had some effect in increasing levels of cleaved Caspase 3 and cleaved PARP, and eliciting apoptotic cell death. However, simultaneous treatment with Bosutinib and knockdown of YAP1 had a synergistic effect on the elevation of cleaved Caspase 3 (Fig. 7H), BAX vs BCL2 ratio (Fig. S7A), cleaved PARP (Fig. S7B). Diminished YAP1 and inhibition of TERT mitochondrial shuttle in IDH1 WT cells triggered apoptosis to a level comparable to Bosutinib treated IDH1 R132H cells (Fig. 7I, Fig. S7C).

Discussion

YAP1 has been indicated to be at the epicenter of signaling networks that serve as major determinant of clinical aggressiveness of tumors and has a strong correlation with patient survival (Rozengurt et al., 2018). C-Jun, a known upstream regulator of YAP1 (Zhang et al., 2020a), was found to be involved in the reduction of YAP1 levels in IDH1 R132H cells. TEADs are the main mediator of YAP1 coactivator activity in YAP1-amplified glioblastoma (Stein et al., 2015), and diminished nuclear TEAD2 together with reduced YAP1 levels was crucial in regulating the transcription of TFAM and TERT in IDH1 R132H. Also, analysis of TCGA data indicated significant decrease in mRNA expressions of well-known YAP1/TEAD responsive genes in IDH1 R132H, thereby suggesting that diminished YAP1/TEAD activity is a feature of IDH1 R132H gliomas. Importantly, we demonstrate for the first time the involvement of YAP1/TEAD2 in regulating TFAM expression. YAP1 dependent decrease in TFAM was accompanied by reduced MFN1 expression, increased mitochondrial DRP1 levels and enhanced mitochondrial fragmentation and ROS generation. As morphological changes in mitochondria are controlled by their dynamics of fission/fusion, increased recruitment of DRP1 to mitochondria and decrease in MFN1 levels could have contributed to enhanced mitochondrial fragmentation in IDH1 R132H by favoring fission over fusion. It is likely that YAP1 mediated decrease in TFAM leads to subsequent reduction in mitochondrial DNA integrity and heightened mtROS in IDH1 mutant glioma.

Diminished TERT in the setting of reduced YAP1 and elevated mtROS was accompanied by its extranuclear shuttle into the mitochondria. TERT inhibition is regarded as a strategy for facilitating induction of the mitochondrial pathway of apoptosis (Massard et al., 2006). Though mitochondrial TERT localization could contribute to increased resistance to oxidative stress in

IDH1 R132H cells by modulating ROS levels (Ahmed et al., 2008); the concomitant reduction in TERT expression could compensate this protective role of TERT in buffering high ROS levels. Inhibition of mitochondrial TERT shuttling induced death in IDH1 WT cells only under conditions of YAP1 deficiency, a condition that prevails in IDH1 R132H to maintain ROS at a heightened basal level. Thus, mitochondrial TERT exerts a protective function against YAP1 deficit-induced oxidative stress in IDH1 R132H glioma cells and removal of this protection enhances sensitivity of IDH1 mutant to ROS generation.

YAP1 mediates resistance in cancer therapies (Lin et al., 2015), and targeting YAP1 has been suggested as a rationale for potential therapeutic interventions (Liu-Chittenden et al., 2012). Importantly, targeting YAP/TEAD protein-protein interaction in GBMs with elevated YAP1 expression has been suggested as a viable therapeutic strategy (Saunders et al., 2021). As IDH1 mutation in glioma patients is a predictor of better responsiveness to drug treatments (Hartmann et al., 2011), the ability of diminished YAP1/TEAD2 levels to dampen TERT and TFAM expressions in these patients support the clinical relevance of our findings. Oxidative stress mediates higher chemosensitivity to cisplatin in IDH1 mutant cancer cells as compared to IDH1 WT cells (Khurshed et al., 2018). Besides, heightened oxidative stress dependent on 2-HG accumulation in IDH1 mutant cancer cells is associated with increased responsiveness to irradiation (Molenaar et al., 2015).

Achieving an effective synergy through combination of chemotherapeutic agents with similar abilities to elevate oxidative stress has been suggested as an efficacious means to inhibit glioma cell growth (Sharma et al., 2007). Bosutinib, a tyrosine kinase inhibitor of the Src/Abl pathway approved for chronic myeloid leukemia, prevents reduction of mitochondrial ROS resulting from TERT accumulation within mitochondria (Miwa et al., 2016). Reduced YAP1 levels in mutant IDH1 determines its resistance to ROS-mediated death stimuli, as Bosutinib-induced ROS generation triggers apoptosis in IDH1 WT cells only under conditions of depleted YAP1 levels. This study not only highlights the non-canonical function of YAP1 in redox regulation, but also suggests that integrating YAP1 inhibitors together with regulators of nuclear-mitochondrial TERT shuttle has important implications for determining the sensitivity of both IDH1 WT and IDH1 R132H cells to ROS stressors. Changes in mitochondrial dynamics and alterations in redox status modulated by YAP1 in IDH1 wild type and mutant gliomas may have clinical relevance pertaining to their sensitivity to targeted therapies.

Materials and Methods

Cell culture and generation of stable cell lines

Human glioma cell lines LN18 (CRL-2610; ATCC, Manassas, VA, USA) and T98G (CRL-1690; ATCC) were grown in Dulbecco's Modified Eagle Medium (12800; Gibco, Carlsbad, CA, USA) supplemented with 10% heat inactivated fetal bovine serum (HI-FBS) (10082147; Gibco) and penicillin (100 U/ml)-streptomycin (100 μg/ml) (15140-122; Gibco). LN18 cells were stably transfected with pEGFP-N1 IDH1 WT and pEGFP-N1 IDH1 R132H constructs (kind gifts from Professor Hai Yan, Duke University School of Medicine, Durham, NC, USA) as described previously (Gowda et al., 2018) to generate stable cell lines, hereafter referred to as IDH1 WT and IDH1 R132H.

Plasmids and site directed mutagenesis

Cloning and PCR-based mutagenesis was done as described previously (Gowda et al., 2021). TFAM promoter (insert; 803 bp) was cloned into pGL3 basic luciferase reporter vector (E1741; Promega) flanked by restriction sites for MluI and BglII. The insert was PCR amplified using One-Step RT-PCR kit (210210; Qiagen). Both the insert and the vector were subjected to restriction digestion using MluI (R0198S; NEB, Ipswich, MA) and BglII (R0144S; NEB) enzymes, ligated overnight using T4 DNA ligase (M0202L; NEB) and transformed into Subcloning Efficiency DH5α Competent Cells (18265017; Invitrogen). Colonies were screened by PCR and cloning was confirmed by Sanger sequencing. The construct was designated as TFAM WT luciferase.

Mutant plasmids were generated by site-directed mutagenesis. The predicted TEAD2 binding site in the TFAM WT luciferase construct (GCCCCGCCCCC) was mutated to GACTGGAGCAC by site-directed mutagenesis by PCR using Phusion High-Fidelity DNA Polymerase (M0530S; NEB). The template DNA was eliminated by treatment with DpnI (R0176S; NEB), the product was purified using QIAquick PCR Purification Kit (28104; Qiagen), and transformed into Subcloning Efficiency DH5α Competent Cells. Similarly, pBABE YAP1 plasmid was mutated to replace serine with alanine at the ninety-fourth position (S94A; TCC to GCG). The mutant contructs were designated as TFAM Δ luciferase and pBABE YAP1-S94A respectively. The constructs were verified by Sanger sequencing.

The sequences of primers used for cloning and mutagenesis are provided in table 1.

Transfections and treatments

T98G, LN18, IDH1 WT and IDH1 R132H cells were seeded into culture dishes 18 hours before transfection and allowed to grow in complete media. The media was replaced with Opti-MEM Reduced Serum Medium (51985034; Gibco) two hours prior to transfection. Cells were transfected with pBABE-puro (Plasmid #1764; Addgene, Watertown, MA, USA), pBABE YAP1 (Plasmid #15682; Addgene), pBABE YAP1-S94A, pEGFP-N1 IDH1 WT, or pEGFP-N1 IDH1 R132H constructs using Lipofectamine 2000 Transfection Reagent (11668-027; Invitrogen, Carlsbad, CA, USA), or with 20 nM non-targeting siRNA (D-001210-03-20; Dharmacon, Lafayette, CO, USA) or 75 nM YAP1 siRNA (L-012200-00-0010; Dharmacon) using Lipofectamine RNAiMAX Transfection Reagent (13778-075; Invitrogen). The cells were allowed to grow for 24 hours, after which they either underwent further treatment or were harvested.
For treatments, the cells were serum-starved for 6 hours. Cells were treated with 10 μM SP600125 (420119; Sigma-Aldrich, St. Louis, MO, USA), 40 mM D-α-Hydroxyglutaric acid disodium salt (H8378; Sigma-Aldrich) for 48 hours, and/or with 5 μM Bosutinib (PZ0192; Sigma-Aldrich) and/or N-Acetyl-L-cysteine (NAC) (A9165; Sigma-Aldrich) for 18 hours. DMSO (D8418; Sigma-Aldrich,) was used as control for Bosutinib treatment. Thereafter, the cells were harvested for further processing.

Protein isolation and western blot analysis

Whole cell and nuclear proteins were extracted from cells as previously described (Gowda et al., 2018). Mitochondria were isolated using Mitochondrial Isolation Kit for Mammalian Cells (89874; Thermo Scientific, Waltham, MA, USA) by reagent-based method according to manufacturer's instructions. The mitochondrial pellets were resuspended and lysed in mitochondrial lysis buffer (MLB) containing 50 mM Tris-HCl, pH 7.4, 150 mM NaCl, 2 mM EDTA, 2 mM EGTA, 0.2% (v/v) Triton X-100, 0.3% (v/v) NP-40, protease inhibitor cocktail and PMSF to isolate mitochondrial proteins (Arnoult et al., 2009). The nuclear pellet obtained during isolation of mitochondria was resuspended and washed in STM buffer containing 250 mM sucrose, 50 mM Tris-HCl, pH 7.4 and 5 mM MgCl2. The pellet was then resuspended in NET buffer containing 20 mM HEPES, pH 7.9, 1.5 mM MgCl2, 0.5 M NaCl, 0.2 mM EDTA, 20%

(v/v) glycerol and 1% (v/v) Triton X-100, incubated on ice for 30 minutes, sonicated, and centrifuged at 9000 x g to obtain nuclear protein extract as the supernatant (Dimauro et al., 2012). Protein concentrations in the various protein extracts were determined using Pierce BCA Protein Assay Kit (23225; Thermo Scientific) according to manufacturer's protocol. Proteins were subjected to electrophoresis and Western blot analysis was performed using antibodies against IDH1 R132H (SAB4200548; Sigma-Aldrich), YAP1 (ab52771; Abcam, Cambridge, UK), c-JUN (sc-1694; Santa Cruz Biotechnology, Dallas, TX, USA), phospho (Ser63) c-JUN (9261; Cell Signaling Technologies, Danvers, MA, USA), JNK (9252, Cell Signaling Technologies), phospho-JNK (4668, Cell Signaling Technologies), TEAD2 (sc-67115; Santa Cruz Biotechnology), TFAM (NBP1-71648; Novus Biologicals, Littleton, CO, USA), MFN1 (ab57602; Abcam), DRP1 (D6C7; Cell Signaling Technologies), TERT (ab94523; Abcam), Caspase-3 (9662; Cell Signaling Technologies**)**, BAX (sc-493; Santa Cruz Biotechnology) and BCL2 (2872; Cell Signaling Technologies), PARP (9532; Cell Signaling Technologies). Antibodies against β-actin (A3854; Sigma-Aldrich), β-tubulin (sc-9104; Santa Cruz Biotechnology), Histone H3 (9715; Cell Signaling Technologies), C23 (sc-55486; Santa Cruz Biotechnology) or COX-IV (4850; Cell Signaling Technologies) were used to determine equivalent loading. Peroxidase-conjugated secondary antibodies were purchased from Vector Laboratories Inc. (Burlingame, CA, USA). Enhanced chemiluminescent HRP substrate (WBKLS0500; Millipore, Billerica, MA, USA) was added and the blots were imaged in Syngene G:Box XX8 system (Syngene, Frederick, MD, USA) using GeneSys software (Syngene, Frederick, MD, USA). Densitometric analyses on the blots were performed using ImageJ. The results were plotted as fold change over control in each case.

Quantitative real-time PCR

Total RNA was isolated from the cells using RNeasy Mini Kit (74104; Qiagen, Hilden, Germany) as per manufacturer's protocol, and cDNA was synthesized using High-Capacity cDNA Reverse Transcription Kit (4368814; Applied Biosystems Inc., Foster City, CA, USA) on ProFlex PCR System thermal cycler (Applied Biosystems Inc.). Relative real-time PCR was performed as described previously (Gowda et al., 2018) using Power SYBR Green PCR Master Mix (4367659; Applied Biosystems Inc.) on QuantStudio 5 Real-Time PCR System (Applied Biosystems Inc.). The results were analysed using the delta delta Ct method and plotted as fold change over control

for each transcript. 18S rRNA was used as the internal control. The sequences of primers used are given in table 1.

Co-immunoprecipitation

Co-immunoprecipitation was performed as previously described (Gowda et al., 2018). Briefly, nuclear protein extracts were incubated with anti-TEAD2 antibody at 4 °C for 16 hours. This was followed by incubation with protein A/G sepharose beads (6503; Bio Vision, Milpitas, CA, USA) at room temperature for 4 hours. The beads were washed with IP buffer, and the immunoprecipitated proteins were subjected to Western blot analysis using antibodies against YAP1 and TEAD2. 10% inputs were also processed along with the immunoprecipitated samples.

Chromatin immunoprecipitation

ChIP was performed as described previously (Gowda et al., 2018). Cells were fixed using 1% formaldehyde. Nuclei were isolated and chromatin was sheared enzymatically using ChIP-IT Express Enzymatic Shearing Kit (53009; Active Motif, Carlsbad, CA, USA). The sheared DNA was immunoprecipitated using anti-TEAD2 or RNA pol II antibody and protein A/G magnetic beads (6527; Bio Vision). ChIP grade Rabbit IgG (ab171870; Abcam) was used as isotype control. The immunoprecipitated DNA and 10% input samples were purified using phenol-chloroform extraction. Real-time PCR was performed and the results were analysed by percent input method. The sequences of primers used for RT-PCR are given in table 1.

TRAP (telomere repeat amplification protocol) assay

TRAP assay was performed using TeloTAGGG Telomerase PCR ELISA kit (11854666910; Roche, Basel, Switzerland) as described previously (Ahmad et al., 2016) according to manufacturer's protocol. Briefly, cells were lysed in the lysis reagent and protein concentration in the samples was estimated. 0.5 μg of protein from each sample was used for the TRAP reaction. Hybridization and ELISA were performed using the PCR product, and absorbance was measured at 450 nm. The relative telomerase activity was determined and expressed as fold change over control.

PCR-based telomere length measurement

Telomere length was measured by quantitative PCR (Cawthon, 2002). DNA was isolated from the cells using QIAamp DNA Mini Kit (51304; Qiagen). 35 ng of DNA was used for each real time PCR reaction, performed using telomere specific primers or primers for single copy gene, 36B4. The average telomere length for each sample was determined indirectly as the T/S ratio, which was calculated as $T/S = [2^{Ct(T)}/2^{Ct(S)}]^{-1} = 2^{-\Delta Ct}$; where, Ct(T) is the Ct value for telomere, Ct(S) is the Ct value for single copy gene 36B4, and ΔCt is the difference between Ct(T) and Ct(S). The results were expressed as T/S values relative to control. The sequences of primers used for RT-PCR are given in table 1.

Quantification of mitochondrial DNA content

Relative mitochondrial DNA content was determined by PCR-based method (Rooney et al., 2015). Total DNA was isolated from the cells using QIAamp DNA Mini Kit (51304; Qiagen) according to manufacturer's protocol, quantified with a spectrophotometer, and diluted to a concentration of 3 ng/μl in TE buffer. Real-time PCR was performed with 6 ng of template DNA using primers for mitochondrial gene ND1 and nuclear gene B2M. Mitochondrial DNA content relative to nuclear DNA content was calculated as ΔCt = Ct(nDNA) – Ct(mtDNA) and Relative mtDNA content = $2 \times 2^{\Delta Ct}$; where, Ct(nDNA) is the Ct value for nuclear gene B2M and Ct(mtDNA) is the Ct value for mitochondrial gene ND1. The results were expressed as fold change in mtDNA content with respect to control. The sequences of primers used for RT-PCR are given in table 1.

Measurement of mitochondrial ROS

Mitochondrial ROS levels in the cells were measured using MitoSOX Red reagent (M36008; Invitrogen). Cells were grown in 96 well plates. The media was removed and cells were washed with PBS. This was followed by incubation with 5 μm MitoSOX Red reagent in PBS at 37 ^{o}C for 25 minutes. Thereafter, the cells were washed with PBS and fluorescence was measured using Infinite M200 Pro microplate reader (TECAN, Männedorf, Switzerland) (Excitation/Emission: 510/580 nm). The fluorescence intensities were expressed as fold change relative to controls.

MTS Assay

Cell viability was determined by MTS assay (G3580; Promega Corporation, Madison, WI) as described previously (Sheikh et al., 2018). Briefly, cells were grown in 96 well plates and subjected to the required treatments. 20 µl of MTS solution was added to each well. After 4 hours of incubation, absorbance was measured at 490 nm. The values were expressed as a percentage relative to controls.

Mitochondrial staining and immunofluorescence

Cells grown in chambered glass slides were washed with PBS, and incubated with 20 nM MitoTracker Deep Red FM (M22426; Invitrogen) in phenol-free DMEM at 37 ^{o}C for 40 minutes. Cells were then washed with phenol-free DMEM and fixed with 4% formaldehyde in PBS. Thereafter, the cells were permeabilized with 0.075% Triton X100 in PBS. For immunostaining, blocking was performed using 2% BSA and 3% serum in PBS. The cells were incubated overnight in primary antibody (TERT; ab94523, Abcam) with 0.1% BSA and 3% serum in PBS at 4 ^{o}C. This was followed by incubation in secondary antibody (Alexa Fluor 488 – Goat anti-rabbit IgG; A11008, Invitrogen) at room temperature for 1.5 hour. After staining, the cells were mounted in Vectashield Antifade Mounting Medium with DAPI (H-1200; Vector Laboratories Inc.).

TUNEL staining

TUNEL staining was performed using In Situ Cell Death Detection Kit, TMR red (12156792910; Roche) as per manufacturer's instructions. Briefly, cells grown in chambered glass slides were washed with PBS and fixed in 4% formaldehyde in PBS. This was followed by permeabilization using 0.1% Triton X100 in 0.1% sodium citrate. TUNEL reaction mix containing enzyme solution and label solution was added and cells were incubated at 37 ^{o}C for 1 hour. The slides were washed with PBS and mounted in Vectashield Antifade Mounting Medium with DAPI.

Immunofluorescence and confocal imaging

Mitochondrial staining and immunofluorescence slides were imaged on Nikon Eclipse Ti2 microscope using 100X 1.4 NA oil immersion objective, at a zoom of 1.5, using Andor Zyla sCMOS camera, controlled by NIS-Elements software. Images were acquired at 2560 x 2160 pixels.

TUNEL stained slides were imaged with Nikon A1R confocal microscope configured with Nikon Eclipse Ti2, controlled by NIS-Elements software. Z-stack images of 1024 x 1024 pixels per frame, with a step size of 1.05 µm, were acquired with 40X 0.95 NA objective, at a scan zoom of 1.241. Line averaging was set to 2 and signals were collected sequentially in two-channel mode.

Image Analysis

Widefield fluorescence images were deconvolved on ImageJ using Regularized Inverse Filter algorithm. The mitochondrial morphologies in the cells under each condition was determined based on their appearance by visual inspection. The mitochondria that were more punctate and disconnected were classified as fragmented, while the ones which had a more interconnected and thread-like appearance were classified as not fragmented. The number of cells with fragmented mitochondria were counted and expressed as percentage of total number of cells in each condition. For colocalization analysis, deconvolved widefield fluorescence images were used. ROIs were created around individual cells of interest in the images. Manders' colocalization coefficient (M1) for each ROI was determined using the ImageJ plugin Coloc2.

Confocal images of TUNEL stained slides were used to count the TUNEL positive cells. The number of TUNEL positive cells were expressed as percentage of total number of cells in each experimental condition.

Immunohistochemistry

Histologically confirmed IDH1 WT and IDH1 mutant glioblastoma patient samples were obtained as per the guidelines of the Institutional Human Ethics Committee of All India Institute of Medical Sciences (AIIMS), New Delhi, India. Formalin fixed paraffin embedded tissue sections were deparaffinized in xylene and rehydrated in graded alcohols. Antigen retrieval was performed in Tris-EDTA-Tween 20 buffer (pH 9.0) for YAP1, and in sodium citrate buffer (pH 6.0) for TFAM, at 100 ^{o}C. Endogenous peroxidase activity was quenched with 1% H_2O_2. The tissues were permeabilized using 0.1% Triton X-100. Blocking was performed in 3% normal goat serum, 1% BSA and 0.05% Triton X-100 for YAP1, and in 3% normal horse serum, 1% BSA and 0.05% Triton X-100 for TFAM. The sections were incubated in rabbit monoclonal antibody to YAP1 (1:50; overnight) or mouse monoclonal antibody to TFAM (1:60; 48 hours) at 4 ^{o}C in a humidified

chamber. This was followed by washes with TBS (YAP1) or PBS (TFAM) after which, the sections were incubated with biotinylated anti-rabbit or anti-mouse secondary antibodies for YAP1 and TFAM respectively, at room temperature in a humidified chamber. Thereafter, the sections were processed with VECTASTAIN Elite ABC-HRP kit (PK-6100; Vector Laboratories Inc.) for YAP1 or with Streptavidin HRP (SA50054; Vector Laboratories Inc.) for TFAM, counterstained with hematoxylin, dehydrated in graded alcohols, cleared in xylene and mounted in DPX.

IHC imaging and analysis

Images were captured with Leica DMRXA2 microscope using Leica Application Suite software. Representative images of 4 IDH1 WT tumors and 3 IDH1 mutants tumors each were used for quantitative evaluation of IHC signals of YAP1 and TFAM. Quantification was performed in an automated manner using IHC profiler plugin for ImageJ (Varghese et al., 2014). Staining intensities in the images were classified into four categories by the plugin: 0, negative staining; 1, low positive staining; 2, positive staining and 3, high positive staining. H-scores were calculated as (3 x % of high positive) + (2 x % of positive) + (1 x % of low positive).

Promoter Luciferase Reporter Assays

Luciferase reporter assays were performed using cells transfected with different combinations of plasmids. IDH1 WT and IDH1 R132H cells were grown in 24 well culture plates, and transfected with 500 ng of 8xGTIIC construct (#34615; Addgene) using Lipofectamine 2000 Transfection Reagent, or 500 ng TFAM WT or TFAM Δ luciferase constructs using Lipofectamine 3000 Reagent (L3000015; Invitrogen) along with 20 ng of Renilla luciferase vector, pRL-TK (E2241; Promega) for normalization of transfection efficiency. Cells were lysed and analysed using the Dual-Luciferase Reporter Assay System (E1960; Promega) on GloMax Explorer Multimode Microplate Reader (Promega).

TCGA data analysis

TCGA data for mRNA expression (RNA Seq V2 RSEM) of the genes of interest from low grade glioma (LGG) and glioblastoma (GBM) datasets were downloaded from cBioPortal. The data was segregated based on the IDH1 mutational status (IDH1 WT and IDH1 R132H), log transformed, and compared by unpaired two-tailed t-test.

Statistical analysis

Statistical analysis was performed using GraphPad Prism. Data are represented as mean ± SEM. Comparisons between two groups were performed using two-tailed Student's t test, unless otherwise indicated. Comparisons among multiple groups were done using one-way ANOVA with Tukey's Multiple Comparison Test. Statistical significance is indicated as *, $p < 0.05$; **, $p < 0.01$; ***, $p < 0.001$ and ****, $p < 0.0001$.

Acknowledgements

We acknowledge the help of Shanker Datt Joshi with immunohistochemistry and technical assistance of Rajesh Kumar Kumawat. Reagents and antibodies gifted by Dr. Rajender Motiani, Regional Centre for Biotechnology, Faridabad; and Dr. Pankaj Seth from National Brain Research Centre are acknowledged.

Conflict of Interest

The authors declare that they have no competing interests.

Funding Information

This work was supported by a research grant from the Department of Biotechnology (DBT) (Government of India grant no. BT/Med/30/SP11016/2015) to E.S.

Author Contributions

Conceptualization: SP and ES; Investigation: SP, PG and KL; Validation: SP, PG and KL; Formal analysis: SP; Visualization: SP and ES; Writing: SP and ES; Review and editing: SP, PG, KL and ES; Project administration, supervision and funding acquisition: ES

References

AHMAD, F., DIXIT, D., SHARMA, V., KUMAR, A., JOSHI, S. D., SARKAR, C. & SEN, E. 2016. Nrf2-driven TERT regulates pentose phosphate pathway in glioblastoma. *Cell Death Dis,* 7**,** e2213.

AHMED, S., PASSOS, J. F., BIRKET, M. J., BECKMANN, T., BRINGS, S., PETERS, H., BIRCH-MACHIN, M. A., VON ZGLINICKI, T. & SARETZKI, G. 2008. Telomerase does not counteract telomere shortening but protects mitochondrial function under oxidative stress. *J Cell Sci,* 121**,** 1046-53.

ARNOULT, D., SOARES, F., TATTOLI, I., CASTANIER, C., PHILPOTT, D. J. & GIRARDIN, S. E. 2009. An N-terminal addressing sequence targets NLRX1 to the mitochondrial matrix. *J Cell Sci,* 122**,** 3161-8.

BLASCO, M. A. 2005. Telomeres and human disease: ageing, cancer and beyond. *Nat Rev Genet,* 6**,** 611-22.

BLEEKER, F. E., ATAI, N. A., LAMBA, S., JONKER, A., RIJKEBOER, D., BOSCH, K. S., TIGCHELAAR, W., TROOST, D., VANDERTOP, W. P., BARDELLI, A. & VAN NOORDEN, C. J. 2010. The prognostic IDH1(R132) mutation is associated with reduced NADP+-dependent IDH activity in glioblastoma. *Acta Neuropathol,* 119**,** 487-94.

CAMPBELL, C. T., KOLESAR, J. E. & KAUFMAN, B. A. 2012. Mitochondrial transcription factor A regulates mitochondrial transcription initiation, DNA packaging, and genome copy number. *Biochim Biophys Acta,* 1819**,** 921-9.

CAWTHON, R. M. 2002. Telomere measurement by quantitative PCR. *Nucleic Acids Res,* 30**,** e47.

DANG, L., WHITE, D. W., GROSS, S., BENNETT, B. D., BITTINGER, M. A., DRIGGERS, E. M., FANTIN, V. R., JANG, H. G., JIN, S., KEENAN, M. C., MARKS, K. M., PRINS, R. M., WARD, P. S., YEN, K. E., LIAU, L. M., RABINOWITZ, J. D., CANTLEY, L. C., THOMPSON, C. B., VANDER HEIDEN, M. G. & SU, S. M. 2009. Cancer-associated IDH1 mutations produce 2-hydroxyglutarate. *Nature,* 462**,** 739-44.

DIMAURO, I., PEARSON, T., CAPOROSSI, D. & JACKSON, M. J. 2012. A simple protocol for the subcellular fractionation of skeletal muscle cells and tissue. *BMC Res Notes,* 5**,** 513.

DONG, J., FELDMANN, G., HUANG, J., WU, S., ZHANG, N., COMERFORD, S. A., GAYYED, M. F., ANDERS, R. A., MAITRA, A. & PAN, D. 2007. Elucidation of a universal size-control mechanism in Drosophila and mammals. *Cell,* 130**,** 1120-33.

EKSTRAND, M. I., FALKENBERG, M., RANTANEN, A., PARK, C. B., GASPARI, M., HULTENBY, K., RUSTIN, P., GUSTAFSSON, C. M. & LARSSON, N. G. 2004. Mitochondrial transcription factor A regulates mtDNA copy number in mammals. *Hum Mol Genet,* 13**,** 935-44.

FARRE, D., ROSET, R., HUERTA, M., ADSUARA, J. E., ROSELLO, L., ALBA, M. M. & MESSEGUER, X. 2003. Identification of patterns in biological sequences at the ALGGEN server: PROMO and MALGEN. *Nucleic Acids Res,* 31**,** 3651-3.

GARRETT, M., SPERRY, J., BRAAS, D., YAN, W., LE, T. M., MOTTAHEDEH, J., LUDWIG, K., ESKIN, A., QIN, Y., LEVY, R., BREUNIG, J. J., PAJONK, F., GRAEBER, T. G., RADU, C. G., CHRISTOFK, H., PRINS, R. M., LAI, A., LIAU, L. M., COPPOLA, G. & KORNBLUM, H. I. 2018. Metabolic characterization of isocitrate

dehydrogenase (IDH) mutant and IDH wildtype gliomaspheres uncovers cell type-specific vulnerabilities. *Cancer Metab,* 6**,** 4.
GIAMPAZOLIAS, E. & TAIT, S. W. 2016. Mitochondria and the hallmarks of cancer. *FEBS J,* 283**,** 803-14.
GOWDA, P., LATHORIA, K., SHARMA, S., PATRICK, S., UMDOR, S. B. & SEN, E. 2021. Rewiring of lactate-IL-1beta auto-regulatory loop with Clock-Bmal1: A feed-forward circuit in glioma. *Mol Cell Biol***,** MCB0044920.
GOWDA, P., PATRICK, S., SINGH, A., SHEIKH, T. & SEN, E. 2018. Mutant Isocitrate Dehydrogenase 1 Disrupts PKM2-beta-Catenin-BRG1 Transcriptional Network-Driven CD47 Expression. *Mol Cell Biol,* 38.
GUICHET, P. O., MASLIANTSEV, K., TACHON, G., PETROPOULOS, C., GODET, J., LARRIEU, D., MILIN, S., WAGER, M. & KARAYAN-TAPON, L. 2018. Fatal correlation between YAP1 expression and glioma aggressiveness: clinical and molecular evidence. *J Pathol,* 246**,** 205-216.
HAENDELER, J., DROSE, S., BUCHNER, N., JAKOB, S., ALTSCHMIED, J., GOY, C., SPYRIDOPOULOS, I., ZEIHER, A. M., BRANDT, U. & DIMMELER, S. 2009. Mitochondrial telomerase reverse transcriptase binds to and protects mitochondrial DNA and function from damage. *Arterioscler Thromb Vasc Biol,* 29**,** 929-35.
HARTMANN, C., HENTSCHEL, B., TATAGIBA, M., SCHRAMM, J., SCHNELL, O., SEIDEL, C., STEIN, R., REIFENBERGER, G., PIETSCH, T., VON DEIMLING, A., LOEFFLER, M., WELLER, M. & GERMAN GLIOMA, N. 2011. Molecular markers in low-grade gliomas: predictive or prognostic? *Clin Cancer Res,* 17**,** 4588-99.
HU, W., MA, S. L., LIU, L. L., ZHU, Y. H., ZENG, T. T., LI, Y. & GUAN, X. Y. 2020. Impact of mitochondrial transcription factor A expression on the outcomes of ovarian, endometrial and cervical cancers. *Am J Transl Res,* 12**,** 5343-5361.
IMOTO, M., TACHIBANA, I. & URRUTIA, R. 1998. Identification and functional characterization of a novel human protein highly related to the yeast dynamin-like GTPase Vps1p. *J Cell Sci,* 111 (Pt 10)**,** 1341-9.
ISHIHARA, N., EURA, Y. & MIHARA, K. 2004. Mitofusin 1 and 2 play distinct roles in mitochondrial fusion reactions via GTPase activity. *J Cell Sci,* 117**,** 6535-46.
KHURSHED, M., AARNOUDSE, N., HULSBOS, R., HIRA, V. V. V., VAN LAARHOVEN, H. W. M., WILMINK, J. W., MOLENAAR, R. J. & VAN NOORDEN, C. J. F. 2018. IDH1-mutant cancer cells are sensitive to cisplatin and an IDH1-mutant inhibitor counteracts this sensitivity. *FASEB J***,** fj201800547R.
KONSAVAGE, W. M., JR., KYLER, S. L., RENNOLL, S. A., JIN, G. & YOCHUM, G. S. 2012. Wnt/beta-catenin signaling regulates Yes-associated protein (YAP) gene expression in colorectal carcinoma cells. *J Biol Chem,* 287**,** 11730-9.
LEE, Y., KOH, J., KIM, S. I., WON, J. K., PARK, C. K., CHOI, S. H. & PARK, S. H. 2017. The frequency and prognostic effect of TERT promoter mutation in diffuse gliomas. *Acta Neuropathol Commun,* 5**,** 62.
LI, F., HE, X., YE, D., LIN, Y., YU, H., YAO, C., HUANG, L., ZHANG, J., WANG, F., XU, S., WU, X., LIU, L., YANG, C., SHI, J., HE, X., LIU, J., QU, Y., GUO, F., ZHAO, J., XU, W. & ZHAO, S. 2015. NADP(+)-IDH Mutations Promote Hypersuccinylation that Impairs Mitochondria Respiration and Induces Apoptosis Resistance. *Mol Cell,* 60**,** 661-75.

LIN, L., SABNIS, A. J., CHAN, E., OLIVAS, V., CADE, L., PAZARENTZOS, E., ASTHANA, S., NEEL, D., YAN, J. J., LU, X., PHAM, L., WANG, M. M., KARACHALIOU, N., CAO, M. G., MANZANO, J. L., RAMIREZ, J. L., TORRES, J. M., BUTTITTA, F., RUDIN, C. M., COLLISSON, E. A., ALGAZI, A., ROBINSON, E., OSMAN, I., MUNOZ-COUSELO, E., CORTES, J., FREDERICK, D. T., COOPER, Z. A., MCMAHON, M., MARCHETTI, A., ROSELL, R., FLAHERTY, K. T., WARGO, J. A. & BIVONA, T. G. 2015. The Hippo effector YAP promotes resistance to RAF- and MEK-targeted cancer therapies. *Nat Genet,* 47**,** 250-6.

LIU-CHITTENDEN, Y., HUANG, B., SHIM, J. S., CHEN, Q., LEE, S. J., ANDERS, R. A., LIU, J. O. & PAN, D. 2012. Genetic and pharmacological disruption of the TEAD-YAP complex suppresses the oncogenic activity of YAP. *Genes Dev,* 26**,** 1300-5.

MAMMOTO, A., MUYLEART, M., KADLEC, A., GUTTERMAN, D. & MAMMOTO, T. 2018. YAP1-TEAD1 signaling controls angiogenesis and mitochondrial biogenesis through PGC1alpha. *Microvasc Res,* 119**,** 73-83.

MASSARD, C., ZERMATI, Y., PAULEAU, A. L., LAROCHETTE, N., METIVIER, D., SABATIER, L., KROEMER, G. & SORIA, J. C. 2006. hTERT: a novel endogenous inhibitor of the mitochondrial cell death pathway. *Oncogene,* 25**,** 4505-14.

MEI, H., SUN, S., BAI, Y., CHEN, Y., CHAI, R. & LI, H. 2015. Reduced mtDNA copy number increases the sensitivity of tumor cells to chemotherapeutic drugs. *Cell Death Dis,* 6**,** e1710.

MIWA, S., CZAPIEWSKI, R., WAN, T., BELL, A., HILL, K. N., VON ZGLINICKI, T. & SARETZKI, G. 2016. Decreased mTOR signalling reduces mitochondrial ROS in brain via accumulation of the telomerase protein TERT within mitochondria. *Aging (Albany NY),* 8**,** 2551-2567.

MOLENAAR, R. J., BOTMAN, D., SMITS, M. A., HIRA, V. V., VAN LITH, S. A., STAP, J., HENNEMAN, P., KHURSHED, M., LENTING, K., MUL, A. N., DIMITRAKOPOULOU, D., VAN DRUNEN, C. M., HOEBE, R. A., RADIVOYEVITCH, T., WILMINK, J. W., MACIEJEWSKI, J. P., VANDERTOP, W. P., LEENDERS, W. P., BLEEKER, F. E. & VAN NOORDEN, C. J. 2015. Radioprotection of IDH1-Mutated Cancer Cells by the IDH1-Mutant Inhibitor AGI-5198. *Cancer Res,* 75**,** 4790-802.

NAGARAJ, R., GURURAJA-RAO, S., JONES, K. T., SLATTERY, M., NEGRE, N., BRAAS, D., CHRISTOFK, H., WHITE, K. P., MANN, R. & BANERJEE, U. 2012. Control of mitochondrial structure and function by the Yorkie/YAP oncogenic pathway. *Genes Dev,* 26**,** 2027-37.

ORR, B. A., BAI, H., ODIA, Y., JAIN, D., ANDERS, R. A. & EBERHART, C. G. 2011. Yes-associated protein 1 is widely expressed in human brain tumors and promotes glioblastoma growth. *J Neuropathol Exp Neurol,* 70**,** 568-77.

OUYANG, T., MENG, W., LI, M., HONG, T. & ZHANG, N. 2020. Recent Advances of the Hippo/YAP Signaling Pathway in Brain Development and Glioma. *Cell Mol Neurobiol,* 40**,** 495-510.

PARSONS, D. W., JONES, S., ZHANG, X., LIN, J. C., LEARY, R. J., ANGENENDT, P., MANKOO, P., CARTER, H., SIU, I. M., GALLIA, G. L., OLIVI, A., MCLENDON, R., RASHEED, B. A., KEIR, S., NIKOLSKAYA, T., NIKOLSKY, Y., BUSAM, D. A., TEKLEAB, H., DIAZ, L. A., JR., HARTIGAN, J., SMITH, D. R., STRAUSBERG, R. L., MARIE, S. K., SHINJO, S. M., YAN, H., RIGGINS, G. J., BIGNER, D. D., KARCHIN, R., PAPADOPOULOS, N., PARMIGIANI, G., VOGELSTEIN, B., VELCULESCU, V. E. & KINZLER, K. W. 2008. An integrated genomic analysis of human glioblastoma multiforme. *Science,* 321**,** 1807-12.

PICCA, A. & LEZZA, A. M. 2015. Regulation of mitochondrial biogenesis through TFAM-mitochondrial DNA interactions: Useful insights from aging and calorie restriction studies. *Mitochondrion,* 25**,** 67-75.

QIAN, W., KUMAR, N., ROGINSKAYA, V., FOUQUEREL, E., OPRESKO, P. L., SHIVA, S., WATKINS, S. C., KOLODIEZNYI, D., BRUCHEZ, M. P. & VAN HOUTEN, B. 2019. Chemoptogenetic damage to mitochondria causes rapid telomere dysfunction. *Proc Natl Acad Sci U S A,* 116**,** 18435-18444.

ROONEY, J. P., RYDE, I. T., SANDERS, L. H., HOWLETT, E. H., COLTON, M. D., GERM, K. E., MAYER, G. D., GREENAMYRE, J. T. & MEYER, J. N. 2015. PCR based determination of mitochondrial DNA copy number in multiple species. *Methods Mol Biol,* 1241**,** 23-38.

ROZENGURT, E., SINNETT-SMITH, J. & EIBL, G. 2018. Yes-associated protein (YAP) in pancreatic cancer: at the epicenter of a targetable signaling network associated with patient survival. *Signal Transduct Target Ther,* 3**,** 11.

SAHIN, E., COLLA, S., LIESA, M., MOSLEHI, J., MULLER, F. L., GUO, M., COOPER, M., KOTTON, D., FABIAN, A. J., WALKEY, C., MASER, R. S., TONON, G., FOERSTER, F., XIONG, R., WANG, Y. A., SHUKLA, S. A., JASKELIOFF, M., MARTIN, E. S., HEFFERNAN, T. P., PROTOPOPOV, A., IVANOVA, E., MAHONEY, J. E., KOST-ALIMOVA, M., PERRY, S. R., BRONSON, R., LIAO, R., MULLIGAN, R., SHIRIHAI, O. S., CHIN, L. & DEPINHO, R. A. 2011. Telomere dysfunction induces metabolic and mitochondrial compromise. *Nature,* 470**,** 359-65.

SAUNDERS, J. T., HOLMES, B., BENAVIDES-SERRATO, A., KUMAR, S., NISHIMURA, R. N. & GERA, J. 2021. Targeting the YAP-TEAD interaction interface for therapeutic intervention in glioblastoma. *J Neurooncol,* 152**,** 217-231.

SHARMA, V., JOSEPH, C., GHOSH, S., AGARWAL, A., MISHRA, M. K. & SEN, E. 2007. Kaempferol induces apoptosis in glioblastoma cells through oxidative stress. *Mol Cancer Ther,* 6**,** 2544-53.

SHEIKH, T., GUPTA, P., GOWDA, P., PATRICK, S. & SEN, E. 2018. Hexokinase 2 and nuclear factor erythroid 2-related factor 2 transcriptionally coactivate xanthine oxidoreductase expression in stressed glioma cells. *J Biol Chem,* 293**,** 4767-4777.

SHI, J., SUN, B., SHI, W., ZUO, H., CUI, D., NI, L. & CHEN, J. 2015. Decreasing GSH and increasing ROS in chemosensitivity gliomas with IDH1 mutation. *Tumour Biol,* 36**,** 655-62.

STEIN, C., BARDET, A. F., ROMA, G., BERGLING, S., CLAY, I., RUCHTI, A., AGARINIS, C., SCHMELZLE, T., BOUWMEESTER, T., SCHUBELER, D. & BAUER, A. 2015. YAP1 Exerts Its Transcriptional Control via TEAD-Mediated Activation of Enhancers. *PLoS Genet,* 11**,** e1005465.

VARGHESE, F., BUKHARI, A. B., MALHOTRA, R. & DE, A. 2014. IHC Profiler: an open source plugin for the quantitative evaluation and automated scoring of immunohistochemistry images of human tissue samples. *PLoS One,* 9**,** e96801.

WALLACE, D. C. 2012. Mitochondria and cancer. *Nat Rev Cancer,* 12**,** 685-98.

WEI, S., WANG, J., OYINLADE, O., MA, D., WANG, S., KRATZ, L., LAL, B., XU, Q., LIU, S., SHAH, S. R., ZHANG, H., LI, Y., QUINONES-HINOJOSA, A., ZHU, H., HUANG, Z. Y., CHENG, L., QIAN, J. & XIA, S. 2018. Heterozygous IDH1(R132H/WT) created by "single base editing" inhibits human astroglial cell growth by downregulating YAP. *Oncogene,* 37**,** 5160-5174.

WOO, D. K., GREEN, P. D., SANTOS, J. H., D'SOUZA, A. D., WALTHER, Z., MARTIN, W. D., CHRISTIAN, B. E., CHANDEL, N. S. & SHADEL, G. S. 2012. Mitochondrial genome instability and ROS enhance intestinal tumorigenesis in APC(Min/+) mice. *Am J Pathol,* 180**,** 24-31.

ZHANG, J., WONG, C. C., LEUNG, K. T., WU, F., ZHOU, Y., TONG, J. H. M., CHAN, R. C. K., LI, H., WANG, Y., YAN, H., LIU, L., WU, W. K. K., CHAN, M. W. Y., CHENG, A. S. L., YU, J., WONG, N., LO, K. W., TO, K. F. & KANG, W. 2020a. FGF18-FGFR2 signaling triggers the activation of c-Jun-YAP1 axis to promote carcinogenesis in a subgroup of gastric cancer patients and indicates translational potential. *Oncogene,* 39**,** 6647-6663.

ZHANG, Q., LIU, N., BAI, J., ZHOU, Q., MAO, J., XU, L., LIU, J., WEI, H., REN, C., WU, X., WANG, M., ZHAO, B. & CONG, Y. S. 2020b. Human telomerase reverse transcriptase is a novel target of Hippo-YAP pathway. *FASEB J,* 34**,** 4178-4188.

ZHAO, B., LI, L., LEI, Q. & GUAN, K. L. 2010. The Hippo-YAP pathway in organ size control and tumorigenesis: an updated version. *Genes Dev,* 24**,** 862-74.

ZHAO, B., YE, X., YU, J., LI, L., LI, W., LI, S., YU, J., LIN, J. D., WANG, C. Y., CHINNAIYAN, A. M., LAI, Z. C. & GUAN, K. L. 2008. TEAD mediates YAP-dependent gene induction and growth control. *Genes Dev,* 22**,** 1962-71.

Figures

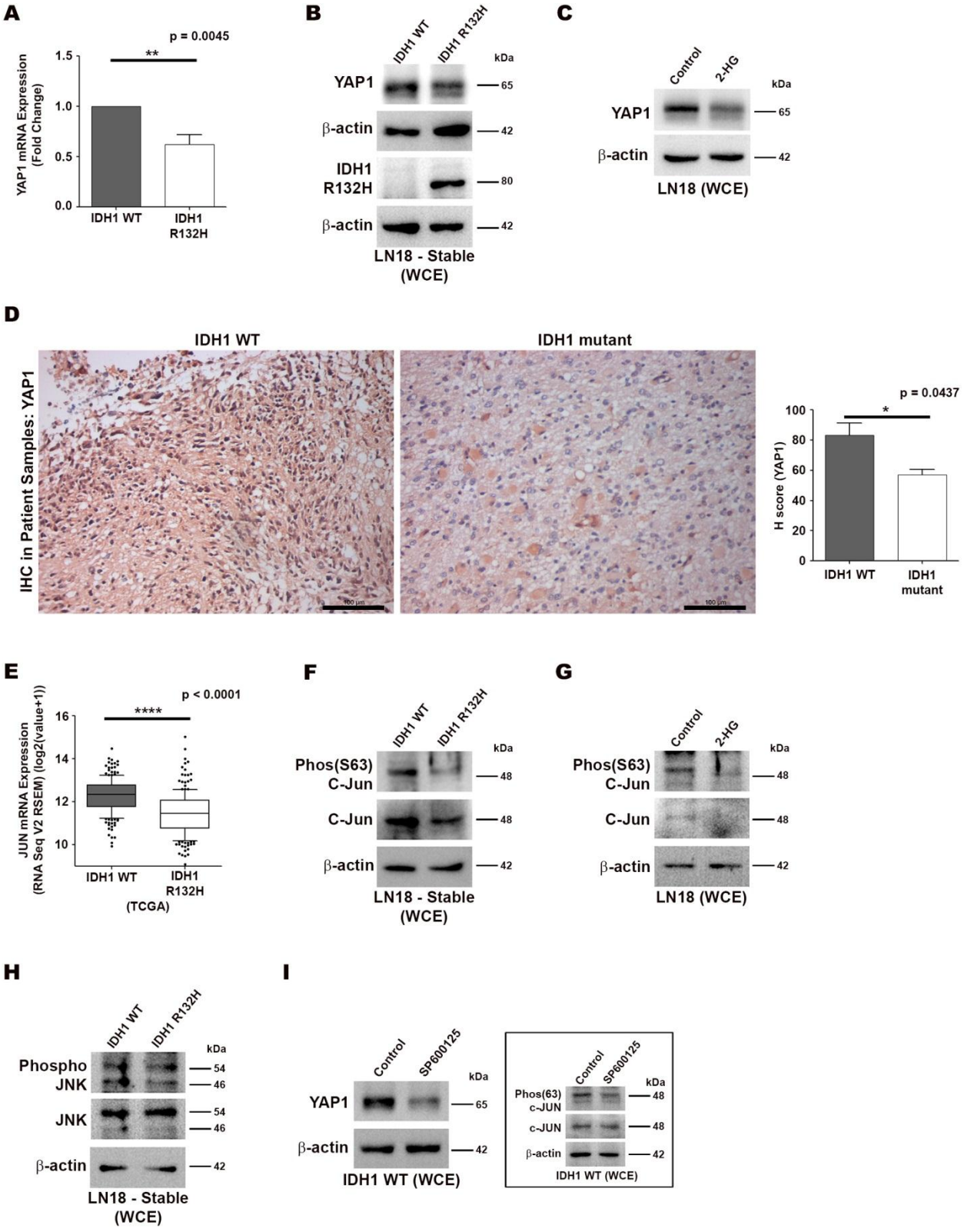

Figure 1. Reduced YAP1 expression in IDH1 R132H

A. qRT-PCR reveals reduced YAP1 mRNA levels in IDH1 R132H cells. Data are expressed as fold change over IDH1 WT and presented as mean ± SEM. N=5 biological replicates. **, $p<0.01$ (Two-tailed student's t-test)
B. Immunoblots show reduced YAP1 levels in IDH1 R132H cells as compared to IDH1 WT cells. The expression of mutant IDH1 R132H in the cells is shown
C. Immunoblots show reduced YAP1 levels in 2-HG-treated LN18 cells
D. Representative images of immunohistochemical staining of patient glioma tissue sections for YAP1 are shown. Scale bar = 100 μm. Quantitative analysis of IHC images shows higher expression of YAP1 in IDH1 WT tumor tissue as compared to IDH1 mutants. Data are presented as mean ± SEM. N=4 IDH1 WT and N=3 IDH1 mutant patients. *, $p<0.05$ (Two-tailed student's t-test)
E. TCGA data analysis shows lower JUN (C-Jun) expression in IDH1 R132H gliomas as compared to IDH1 WT gliomas. Data from N=204 IDH1 WT and 206 IDH1 R132H patients from TCGA have been used for analysis. Whiskers represent 10-90 percentile. ****, $p<0.0001$ (Two-tailed student's t-test)
F. Immunoblots show reduced total C-Jun as well as phosphorylated (Ser63) C-Jun levels in IDH1 R132H cells as compared to IDH1 WT cells
G. Immunoblots show reduced total C-Jun and phosphorylated (Ser63) C-Jun levels in 2-HG-treated LN18 cells
H. Immunoblots show total and phosphorylated JNK levels in IDH1 WT and IDH1 R132H cells
I. Immunoblots show reduced levels of YAP1 in IDH1 WT cells on treatment with SP600125. Inset shows reduction in phosphorylated (Ser63) C-Jun levels in SP600125-treated cells

Immunoblots are representative of N=3 biological replicates. WCE, whole cell extract

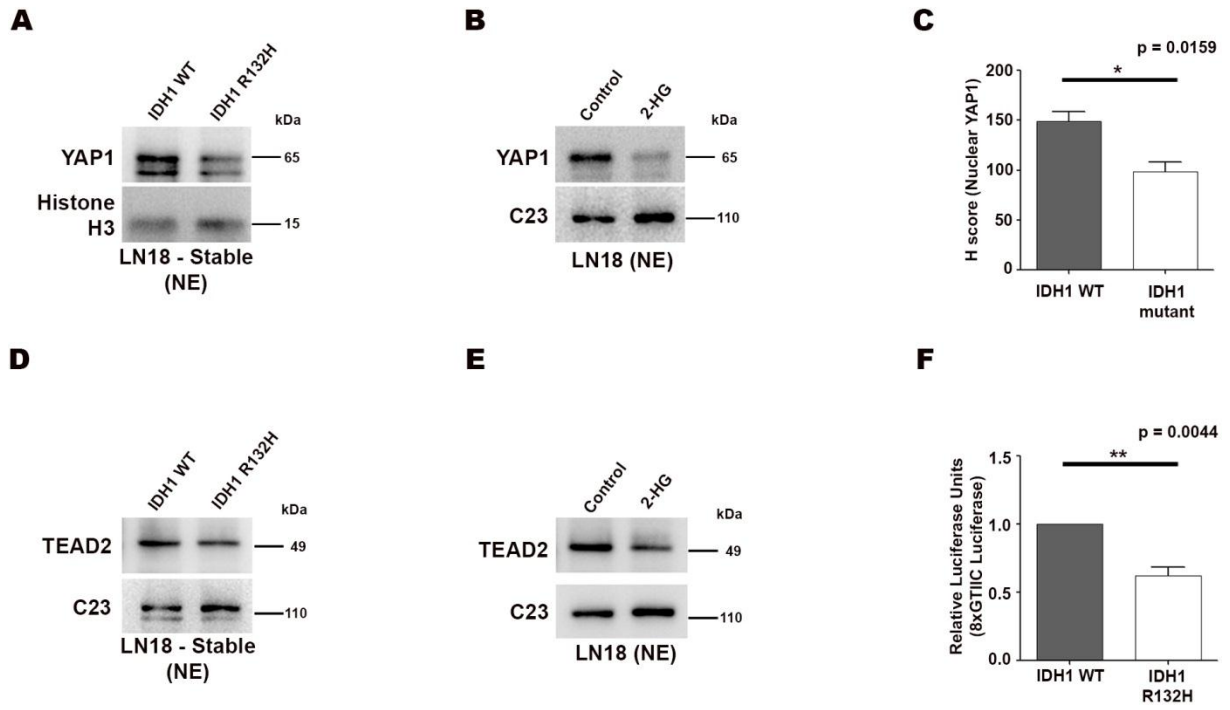

Figure 2. Reduced nuclear YAP1 and TEAD2 in IDH1 R132H cells

A. Immunoblots show diminished nuclear YAP1 levels in IDH1 R132H cells as compared to IDH1 WT

B. Immunoblots show reduced nuclear YAP1 levels in LN18 cells upon treatment with 2-HG

C. Quantitative analysis of YAP1 IHC staining of patient glioma tissue sections shows higher levels of nuclear YAP1 in IDH1 WT tumor tissue as compared to IDH1 mutant. Data are presented as mean ± SEM. N=4 IDH1 WT and N=3 IDH1 mutant patients. *, $p<0.05$ (Two-tailed student's t-test)

D. Immunoblots show decreased nuclear levels of transcription factor TEAD2 in IDH1 R132H cells

E. Decreased nuclear level of TEAD2 in 2-HG-treated LN18 cells is shown by immunoblots

F. 8xGTIIC shows reduced luciferase activity in IDH1 R132H cells as compared to IDH1 WT. Data in relative luciferase units are presented as mean ± SEM. N=3 biological replicates. **, $p<0.01$ (Two-tailed student's t-test)

Immunoblots are representative of N=3 biological replicates (N=2 for 2-HG treatment). NE, nuclear extract

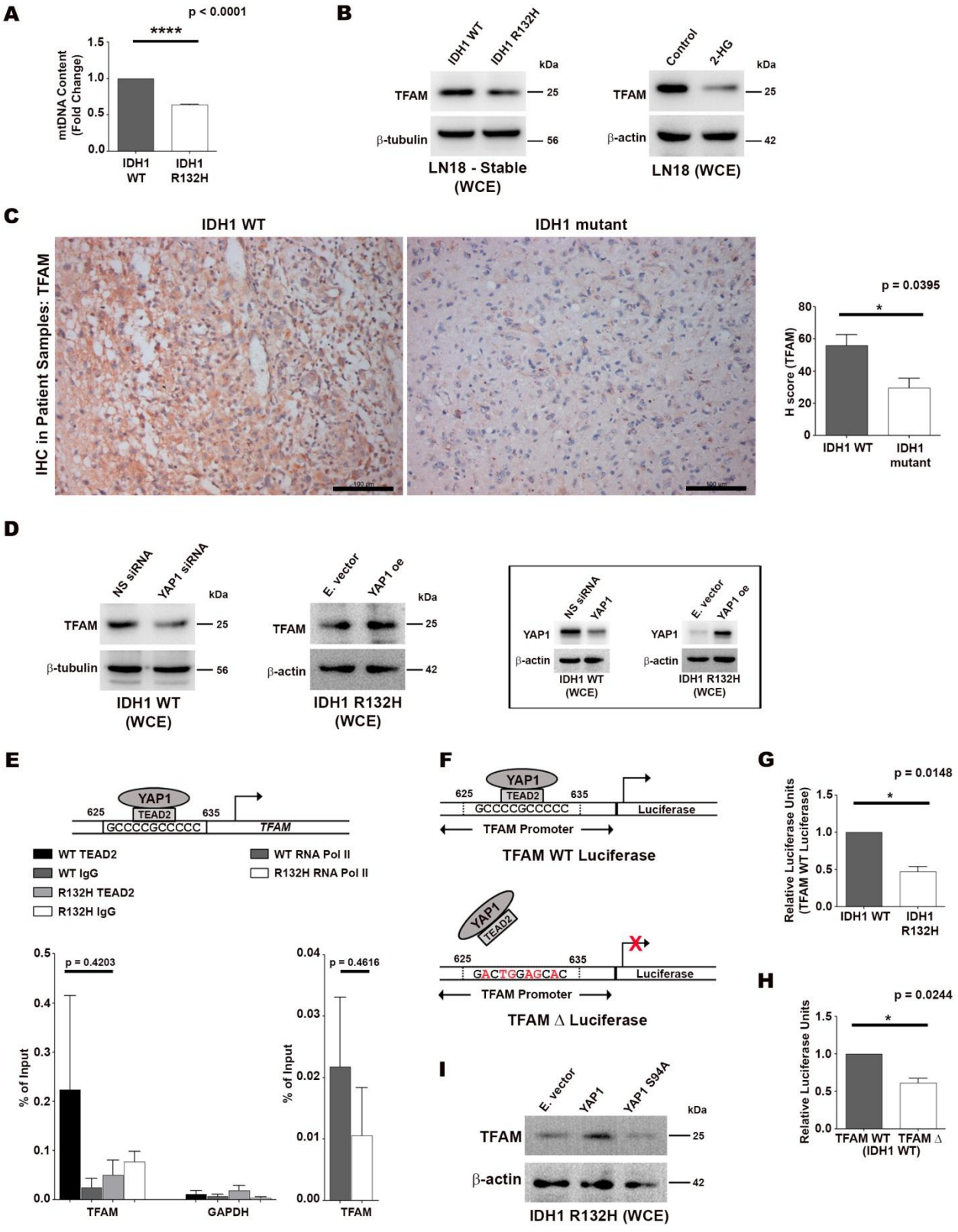

Figure 3. Regulation of TFAM expression by YAP1/TEAD2 complex

A. IDH1 R132H cells show a decrease in mitochondrial DNA (mtDNA) content as determined by qPCR. Data are expressed as fold change over IDH1 WT and presented as mean ± SEM. N=3 biological replicates. *, $p<0.05$ (Two-tailed student's t-test)

B. Immunoblots show reduced levels of TFAM in IDH1 R132H cells and 2-HG-treated LN18 cells as compared to IDH1 WT and control cells respectively

C. Representative images of immunohistochemical staining of patient glioma tissue sections for TFAM are shown. Scale bar = 100 μm. Quantitative analysis of IHC images shows higher expression of TFAM in IDH1 WT tumor tissue as compared to IDH1 mutant. Data are presented as mean ± SEM. N=4 IDH1 WT and N=3 IDH1 mutant patients. *, $p<0.05$ (Two-tailed student's t-test)

D. Reduction in TFAM levels upon siRNA-mediated knockdown of YAP1 in IDH1 WT cells, and increase in TFAM levels on overexpressing YAP1 in IDH1 R132H cells is demonstrated by immunoblots. Knockdown and overexpression of YAP1 are shown in inset.

E. Schematic representation shows the putative TEAD2 binding site on TFAM promoter (position 625 to 635). ChIP-qPCR reveals reduced enrichment of TEAD2 at TFAM promoter in IDH1 R132H compared to IDH1 WT cells. GAPDH promoter is used as negative control. Data expressed as percentage of input are presented as mean ± SEM. N=3 biological replicates. p values from two-tailed student's t-test

F. Schematic representation of TFAM WT (wild type) and TFAM Δ (mutant) promoter luciferase constructs

G. TFAM WT luciferase construct shows reduced luciferase activity in IDH1 R132H cells as compared to IDH1 WT. Data in relative luciferase units are presented as mean ± SEM. N=2 biological replicates. *, $p<0.05$ (Two-tailed student's t-test)

H. TFAM WT luciferase construct shows higher luciferase activity as compared to TFAM Δ luciferase in IDH1 WT cells. Data in relative luciferase units are presented as mean ± SEM. N=2 biological replicates. *, $p<0.05$ (Two-tailed student's t-test)

I. Immunoblots show an increase in TFAM levels on overexpression of wild type YAP1 in IDH1 R132H cells, but not on overexpressing S94A mutant YAP1

Immunoblots are representative of N=3 biological replicates. WCE, whole cell extract; NS siRNA, Non-specific siRNA; E. vector, Empty vector; YAP1 oe, YAP1 overexpression

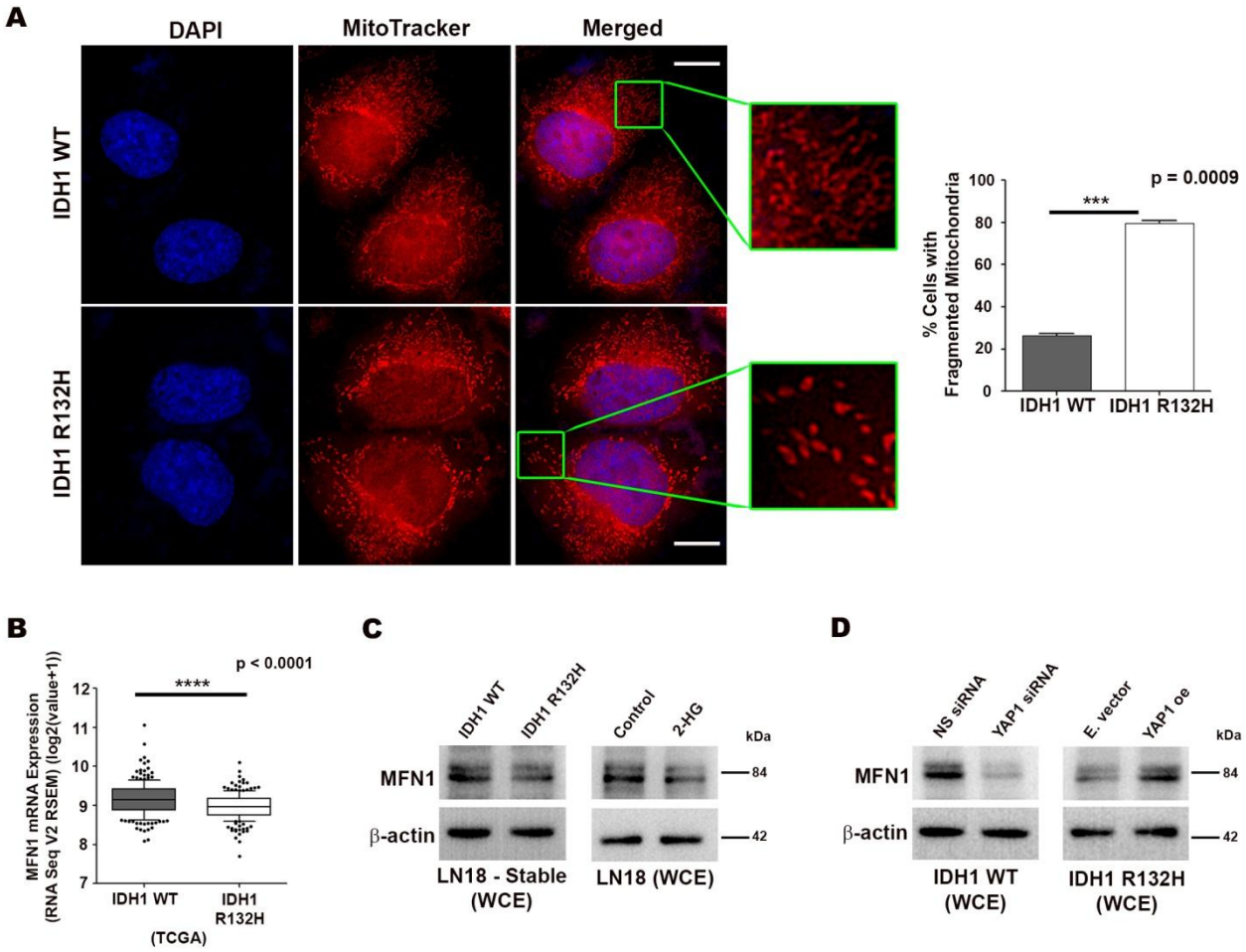

Figure 4. Increased mitochondrial fragmentation in IDH1 R132H

A. Staining with MitoTracker shows elongated mitochondria in IDH1 WT cells while mitochondria in IDH1 R132H cells have a fragmented morphology. Scale bar = 10 μm. Graph shows a higher percentage of cells with fragmented mitochondria in case of IDH1 R132H. Data from ~150 cells under each condition from N=2 biological replicates are presented as mean ± SEM. ***, $p<0.001$ (Two-tailed student's t-test)

B. TCGA data analysis shows lower MFN1 expression in IDH1 R132H gliomas as compared to IDH1 WT gliomas. Data from N=204 IDH1 WT and 206 IDH1 R132H patients from TCGA have been used for analysis. Whiskers represent 10-90 percentile. ****, $p<0.0001$ (Two-tailed student's t-test)

C. Immunoblots show reduced levels of MFN1 in IDH1 R132H cells and 2-HG-treated LN18 cells as compared to IDH1 WT and control cells respectively

D. Immunoblots show reduction in MFN1 levels upon siRNA-mediated knockdown of YAP1 in IDH1 WT cells, and increase in MFN1 levels on overexpressing YAP1 in IDH1 R132H cells

Immunoblots are representative of N=3 biological replicates. WCE, whole cell extract; NS siRNA, Non-specific siRNA; E. vector, Empty vector; YAP1 oe, YAP1 overexpression

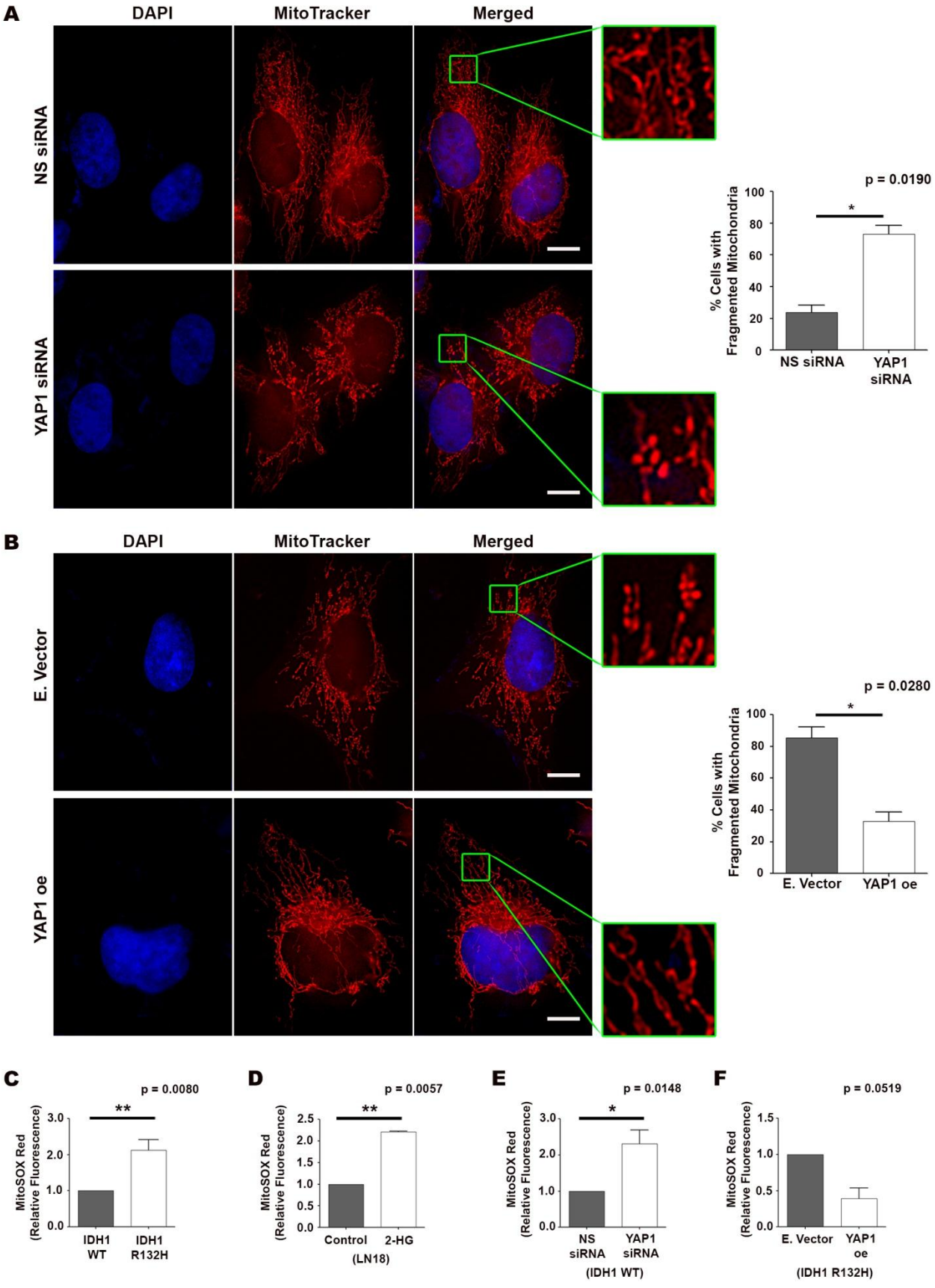

Figure 5. Role of YAP1 in mitochondrial fragmentation and ROS generation

A. Staining with MitoTracker shows elongated mitochondria in IDH1 WT cells transfected with non-specific (NS) siRNA, while mitochondria in IDH1 WT cells transfected with YAP1 siRNA have a more fragmented morphology. Scale bar = 10 μm. Graph shows a higher percentage of YAP1 siRNA-transfected cells with fragmented mitochondria. Data from ~150 cells under each condition from N=2 biological replicates are presented as mean ± SEM. *, $p<0.05$ (Two-tailed student's t-test)

B. Staining with MitoTracker shows fragmented mitochondria in IDH1 R132H cells transfected with empty vector (E. Vector), while mitochondria in IDH1 R132H cells overexpressing YAP1 have a more elongated morphology. Scale bar = 10 μm. Graph shows reduced percentage of YAP1 overexpressing cells with fragmented mitochondria. Data from ~140 cells under each condition from N=2 biological replicates are presented as mean ± SEM. *, $p<0.05$ (Two-tailed student's t-test)

C. MitoSOX Red staining shows elevated levels of mitochondrial ROS in IDH1 R132H cells. Data are expressed as fold change over IDH1 WT and presented as mean ± SEM. N=4 biological replicates. **, $p<0.01$ (Two-tailed student's t-test)

D. MitoSOX Red staining shows increased mitochondrial ROS upon 2-HG treatment in LN18 cells. Data are expressed as fold change over control and presented as mean ± SEM. N=2 biological replicates. **, $p<0.01$ (Paired two-tailed student's t-test)

E. siRNA-mediated knockdown of YAP1 leads to an increase in mitochondrial ROS levels in IDH1 WT cells as shown by MitoSOX Red staining. Data are expressed as fold change over non-specific (NS) siRNA-transfected cells and presented as mean ± SEM. N=4 biological replicates. *, $p<0.05$ (Two-tailed student's t-test)

F. Overexpression of YAP1 leads to a decrease in mitochondrial ROS levels in IDH1 R132H cells as shown by MitoSOX Red staining. Data are expressed as fold change over E. Vector (empty vector)-transfected cells and presented as mean ± SEM. N=2 biological replicates. p value from two-tailed student's t-test

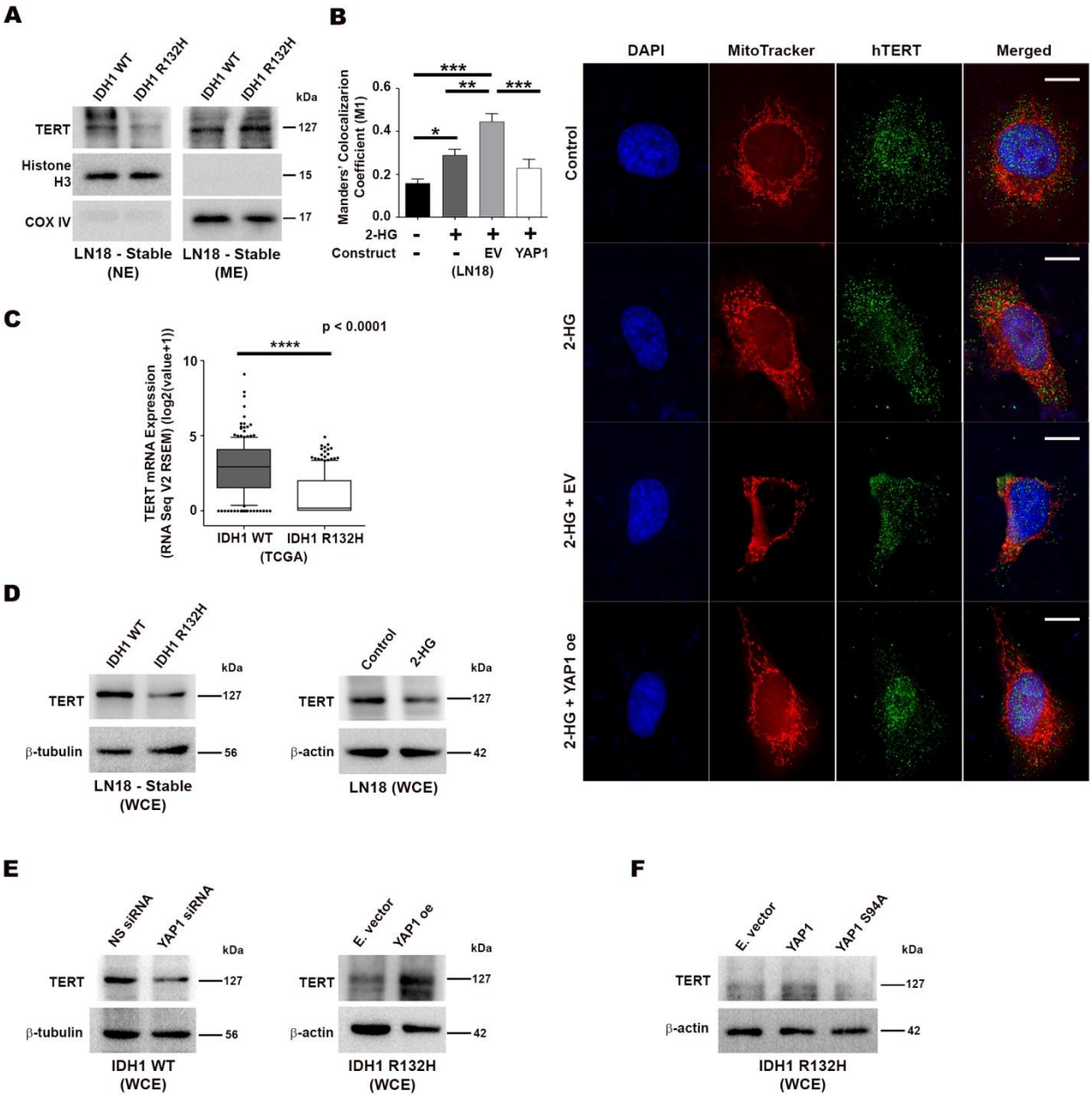

Figure 6. Altered localization and reduced expression of TERT in IDH1 R132H cells

A. Immunoblots demonstrate diminished nuclear levels and increased mitochondrial levels of TERT in IDH1 R132H cells. Blots are representative of N=2 biological replicates. NE, nuclear extract; ME, mitochondrial extract

B. Mitochondrial staining with MitoTracker along with immunostaining shows the localization of TERT under specified conditions. Scale bar = 10 μm. Graph of Manders' colocalization coefficient (M1) shows an increase in mitochondrial localization of TERT upon treatment

with 2-HG. Overexpression of YAP1 in 2-HG-treated cells reduced this mitochondrial localization. Data from 15 cells under each condition from N=2 biological replicates are presented as mean ± SEM. Comparisons between groups were done using One-way ANOVA with Tukey's multiple comparison test. *, $p<0.05$; **, $p<0.01$; ***, $p<0.001$; EV, Empty vector

C. TCGA data analysis shows lower TERT expression in IDH1 R132H gliomas as compared to IDH1 WT gliomas. Data from N=204 IDH1 WT and 206 IDH1 R132H patients have been used for the analysis. Whiskers represent 10-90 percentile. ****, $p<0.0001$ (Two-tailed student's t-test)

D. Immunoblots show reduced levels of TERT in IDH1 R132H cells and 2-HG-treated LN18 cells as compared to IDH1 WT and control cells respectively

E. Immunoblots show a reduction in TERT levels upon siRNA-mediated knockdown of YAP1 in IDH1 WT cells, and an increase in TERT levels on overexpressing YAP1 in IDH1 R132H cells

F. Immunoblots show an increase in TERT levels on overexpression of wild type YAP1 in IDH1 R132H cells, but not on overexpressing S94A mutant YAP1

Immunoblots are representative of N=3 biological replicates (N=2 for mitochondrial and nuclear protein fractions). NE, nuclear extract; ME, mitochondrial extract; WCE, whole cell extract; NS siRNA, Non-specific siRNA; E. Vector, empty vector; YAP1 oe, YAP1 overexpression

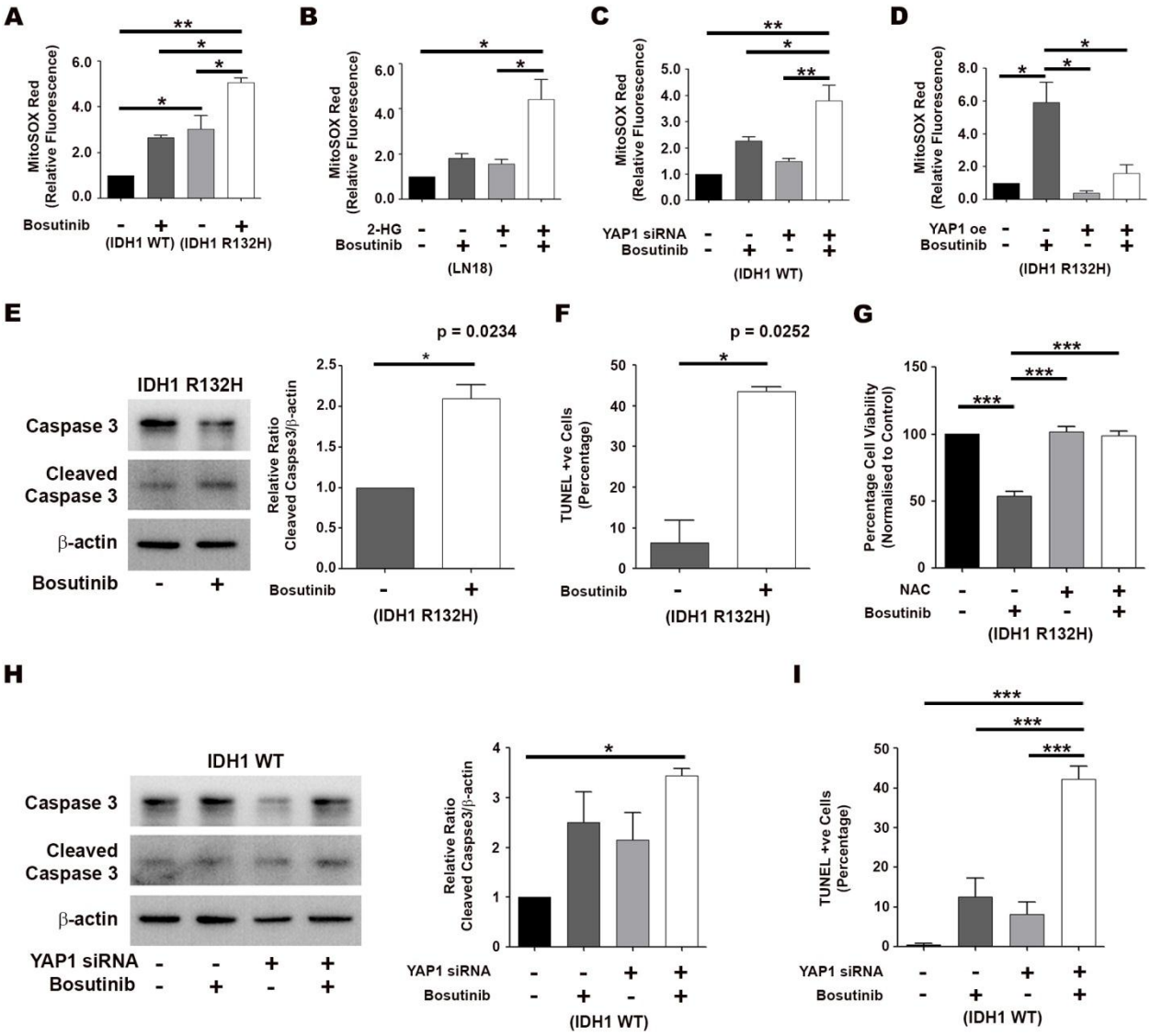

Figure 7. YAP1-dependent susceptibility to ROS and Bosutinib-mediated apoptosis

A. MitoSOX Red staining shows a greater elevation in mitochondrial ROS levels in IDH1 R132H cells upon Bosutinib treatment, as compared to IDH1 WT cells. Data are expressed as fold change over vehicle-treated IDH1 WT cells and presented as mean ± SEM. N=2 biological replicates

B. MitoSOX Red staining shows a greater increase in mitochondrial ROS levels in 2-HG-treated cells as compared to control cells upon Bosutinib treatment. Data are expressed as fold change over vehicle-treated cells and presented as mean ± SEM. N=2 biological replicates

C. Treatment of IDH1 WT cells with Bosutinib along with siRNA-mediated knockdown of YAP1 has a synergistic effect on the elevation of ROS levels in these cells, as shown by MitoSOX Red staining. Data are expressed as fold change over vehicle-treated, non-specific (NS) siRNA -transfected cells and presented as mean ± SEM. N=3 biological replicates

D. Overexpression of YAP1 in IDH1 R132H cells prevents elevation in mitochondrial ROS levels in IDH1 R132H cells upon Bosutinib treatment, as shown by MitoSOX Red staining. Data are expressed as fold change over vehicle-treated IDH1 R132H cells and presented as mean ± SEM. N=2 biological replicates

E. Immunoblot shows increase in levels of cleaved Caspase 3 upon treatment of IDH1 R132H cells with Bosutinib. Graph represents cleaved Caspase 3 levels expressed as fold change over vehicle control, presented as mean ± SEM. N=3 biological replicates. *, $p<0.05$ (Paired two-tailed student's t-test)

F. Treatment with Bosutinib leads to apoptotic death of IDH1 R132H cells, as shown by TUNEL assay. Graph represents the percentage of TUNEL positive cells under each condition, presented as mean ± SEM. N=3 biological replicates. *, $p<0.05$ (Paired two-tailed student's t-test)

G. MTS assay shows that treatment with ROS scavenger NAC (N-acetylcysteine) is sufficient to abrogate Bosutinib-mediated death of IDH1 R132H cells. Cell viability is expressed as percentage normalised to control group and presented as mean ± SEM. N=3 biological replicates.

H. Immunoblots show increase in levels of cleaved Caspase 3 upon Bosutinib treatment along with siRNA-mediated knockdown of YAP1 in IDH1 WT cells. Graph represents cleaved

Caspase 3 levels expressed as fold change over vehicle-treated, non-specific (NS) siRNA-transfected cells, presented as mean ± SEM. N=3 biological replicates

I. Treatment of IDH1 WT cells with Bosutinib along with siRNA-mediated knockdown of YAP1 leads to apoptotic death as shown by TUNEL assay. Graph represents the percentage of TUNEL positive cells under each condition, presented as mean ± SEM. N=3 biological replicates

J. Schematic explaining the role of YAP1 in generation of mitochondrial ROS and TERT-mediated protective effect against oxidative stress in IDH1 WT and IDH1 mutant gliomas

All comparisons among multiple groups were done using One-way ANOVA with Tukey's multiple comparison test. *, $p<0.05$; **, $p<0.01$; ***, $p<0.001$

Table 1: Sequences of primers used in the study. SDM, site directed mutagenesis

	Gene	Primer Sequences
1.	pGL3 TFAM WT (Cloning)	Forward: CGACGCGTTGCTCAAATTAAGCAAGCTG Reverse: GGAAGATCTCGCTCCGGTGGATGAGGCAG
2.	pGL3 TFAM Δ (SDM)	Forward: TCCGCCCCGACTGGAGCACATCTACCGACCGGATGT Reverse: CGGTAGATGTGCTCCAGTCGGGGCGGAATTGGCGCA
3.	pBABE YAP1 S94A (SDM)	Forward: TGCCCGACGCGTTCTTCAAGCCGCCGGA Reverse: TTGAAGAACGCGTCGGGCAGCTTCCGGA
4.	*YAP1*	Forward: GGCGCTCTTCAACGCCGTCATGAAC Reverse: CCTGTCGGGAGTGGGATTT
5.	*TERT*	Forward: GGATGAAGCGGAGTCTGGA Reverse: CGGAAGAGTGTCTGGAGCAA
6.	*TFAM* (ChIP)	Forward: ATTGCGGTTTCCCTTCATCT Reverse: GCCACTAGCGAGGCACTATG
7.	*GAPDH* (ChIP)	Forward: TACTAGCGGTTTTACGGGCG Reverse: TCGAACAGGAGGAGCAGAGAGCGA
8.	Telomere	Forward: GGTTTTTGAGGGTGAGGGTGAGGGTGAGGGTGAGGGT Reverse: TCCCGACTATCCCTATCCCTATCCCTATCCCTATCCCTA
9.	*36B4*/*RPLP0*	Forward: CAGCAAGTGGGAAGGTGTAATCC Reverse: CCCATTCTATCATCAACGGGTACAA
10.	*ND1*	Forward: ACGCCATAAAACTCTTCACCAAAG Reverse: TAGTAGAAGAGCGATGGTGAGAGCTA
11.	*B2M*	Forward: TGCTGTCTCCATGTTTGATGTATCT Reverse: TCTCTGCTCCCCACCTCTAAGT

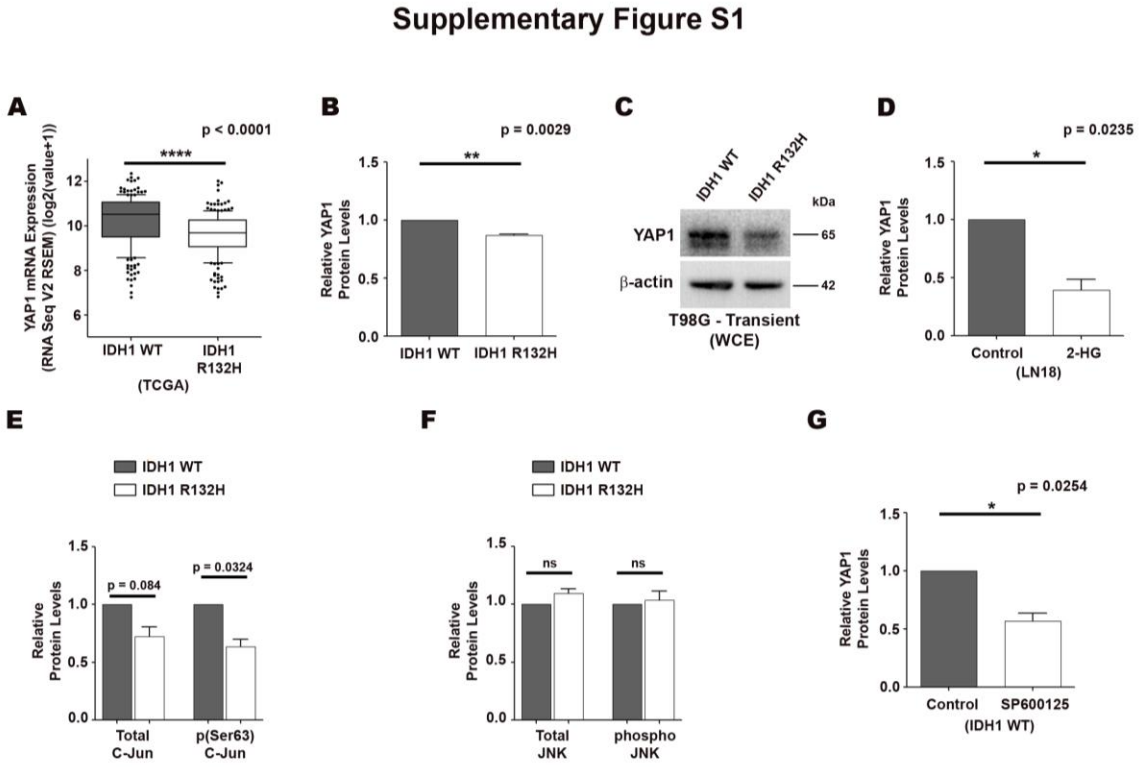

Fig. S1. Reduced YAP1 and C-Jun levels in IDH1 R132H and 2-HG-treated cells

A. RNA expression data from TCGA shows lower YAP1 expression in IDH1 R132H gliomas as compared to IDH1 WT gliomas. Data from N=204 IDH1 WT and 206 IDH1 R132H patients from TCGA have been used for analysis. Whiskers represent 10-90 percentile. ****, p<0.0001 (Two-tailed student's t-test)

B. Densitometric analysis of immunoblots shows lower YAP1 protein levels in IDH1 R132H as compared to IDH1 WT cells

C. Immunoblots show a decrease in YAP1 levels in T98G cells transiently transfected with IDH1 R132H. The blots are representative of two independent experiments with similar results. WCE, whole cell extract

D. Densitometric analysis of immunoblots shows a reduction in YAP1 protein levels in LN18 cells upon 2-HG treatment

E. Densitometric analysis of immunoblots shows a reduction in total and phosphorylated (Ser63) C-Jun protein levels in IDH1 R132H cells
F. Densitometric analysis of immunoblots shows no difference in total and phosphorylated JNK protein levels between IDH1 WT and IDH1 R132H cells
G. Densitometric analysis of immunoblots shows a reduction in YAP1 protein levels on treatment of IDH1 WT cells with SP600125

All densitometry graphs represent data expressed as fold change over respective controls, presented as mean ± SEM. N=3 biological replicates. *, $p<0.05$; **, $p<0.01$. Paired two-tailed student's t-test were used for statistical analysis

Supplementary Figure S2

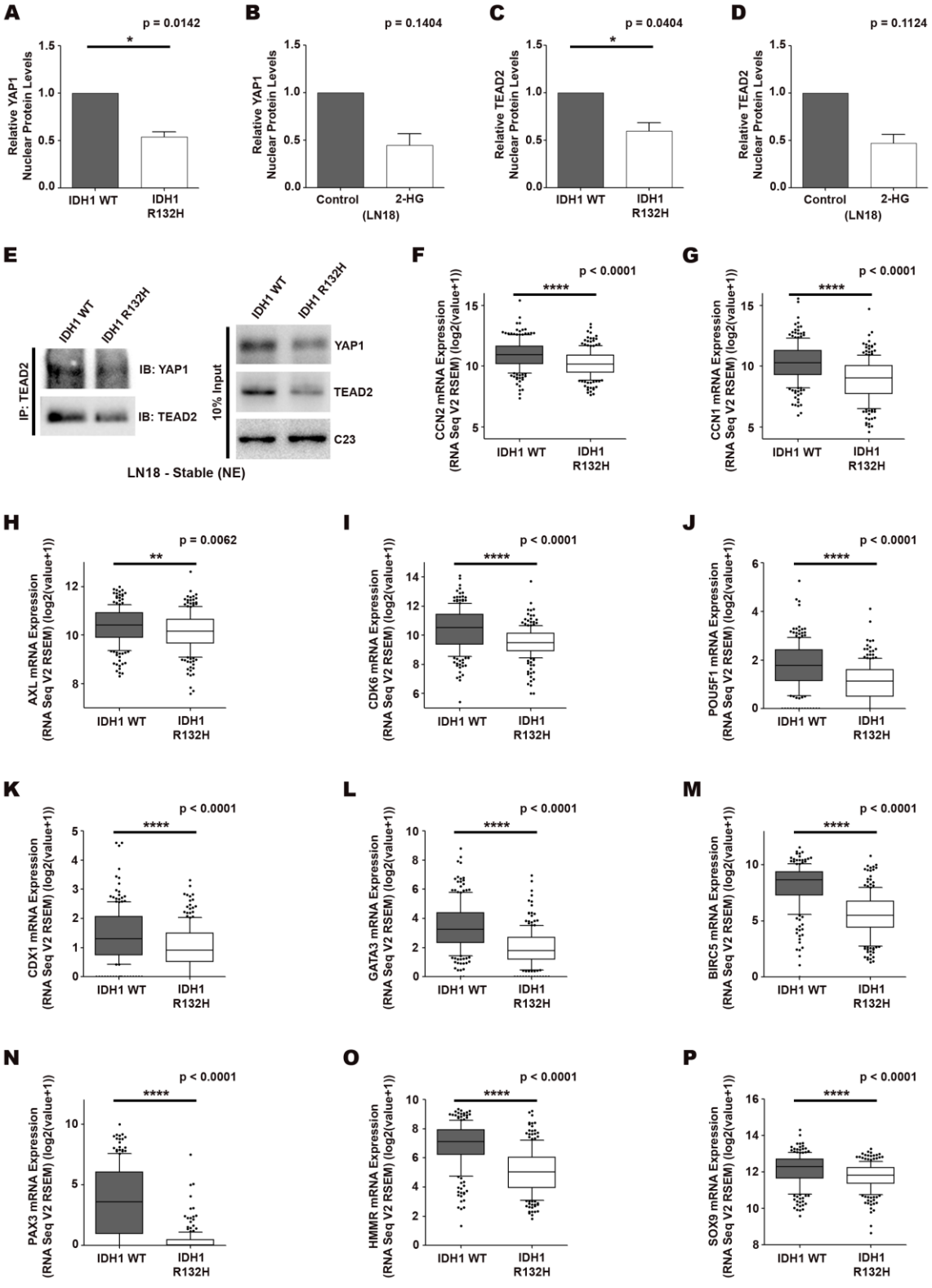

Fig. S2. Reduced Nuclear YAP1 and TEAD2 levels and diminished YAP1/TEAD activity in IDH1 R132H

A. Densitometric analysis shows diminished nuclear YAP1 levels in IDH1 R132H as compared to IDH1 WT cells
B. Densitometric analysis shows a reduction in nuclear YAP1 levels in 2-HG-treated LN18 cells
C. Densitometry shows diminished nuclear TEAD2 levels in IDH1 R132H as compared to IDH1 WT cells
D. Densitometric analysis shows a reduction in nuclear TEAD2 levels upon 2-HG treatment in LN18 cells
E. Coimmunoprecipitation (CoIP) demonstrates reduced YAP1/TEAD2 complex formation in IDH1 R132H cells. The blots are representative of two independent experiments with similar results. NE, nuclear extract

F-P. TCGA data analysis shows lower expression of known TEAD-responsive genes in IDH1 R132H gliomas as compared to IDH1 WT gliomas. Data from N=204 IDH1 WT and 206 IDH1 R132H patients have been used for the analysis. Whiskers represent 10-90 percentile. **, $p<0.01$; ****, $p<0.0001$ (Two-tailed student's t-test)

All densitometry graphs represent data expressed as fold change over respective controls, presented as mean ± SEM. N=3 biological replicates (N=2 biological replicates for nuclear protein levels in 2-HG-treated cells). *, $p<0.05$. Paired two-tailed student's t-test was used for statistical analysis

Supplementary Figure S3

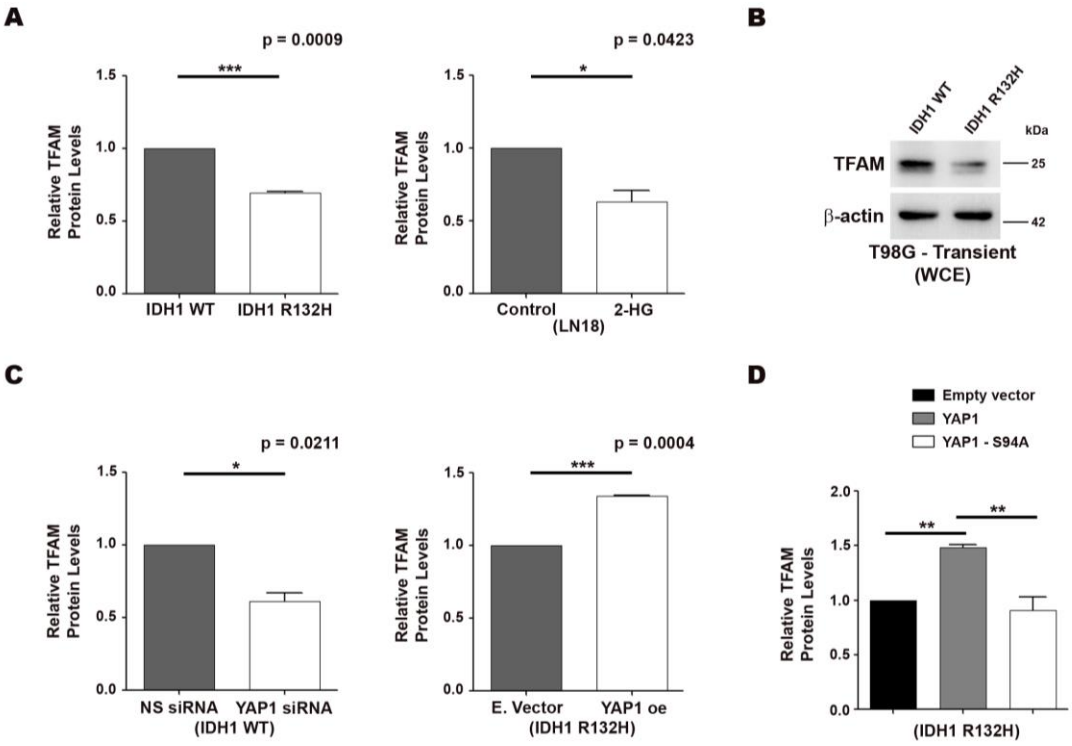

Fig. S3. YAP1-dependent TFAM levels

A. Densitometric analysis of immunoblots shows lower TFAM protein levels in IDH1 R132H cells and 2-HG-treated LN18 cells as compared to IDH1 WT and control cells respectively

B. Immunoblots show a decrease in TFAM levels in T98G cells transiently transfected with IDH1 R132H. The blots are representative of two independent experiments with similar results. WCE, whole cell extract

C. Densitometric analysis shows a reduction in TFAM levels upon siRNA-mediated knockdown of YAP1 in IDH1 WT cells, and an increase in TFAM levels on overexpressing YAP1 in IDH1 R132H cells

D. Densitometric analysis shows an increase in TFAM levels on overexpressing wild type YAP1 in IDH1 R132H cells, but not on overexpressing YAP1-S94A mutant.

All densitometry graphs represent data expressed as fold change over respective controls, presented as mean ± SEM. N=3 biological replicates. *, $p<0.05$; **, $p<0.01$; ***, $p<0.001$. Comparisons between two groups were done using paired two-tailed student's t-test, and comparisons among multiple groups were done using one-way ANOVA with Tukey's multiple comparison test. NS siRNA, Non-specific siRNA; E. vector, Empty vector; YAP1 oe, YAP1 overexpression

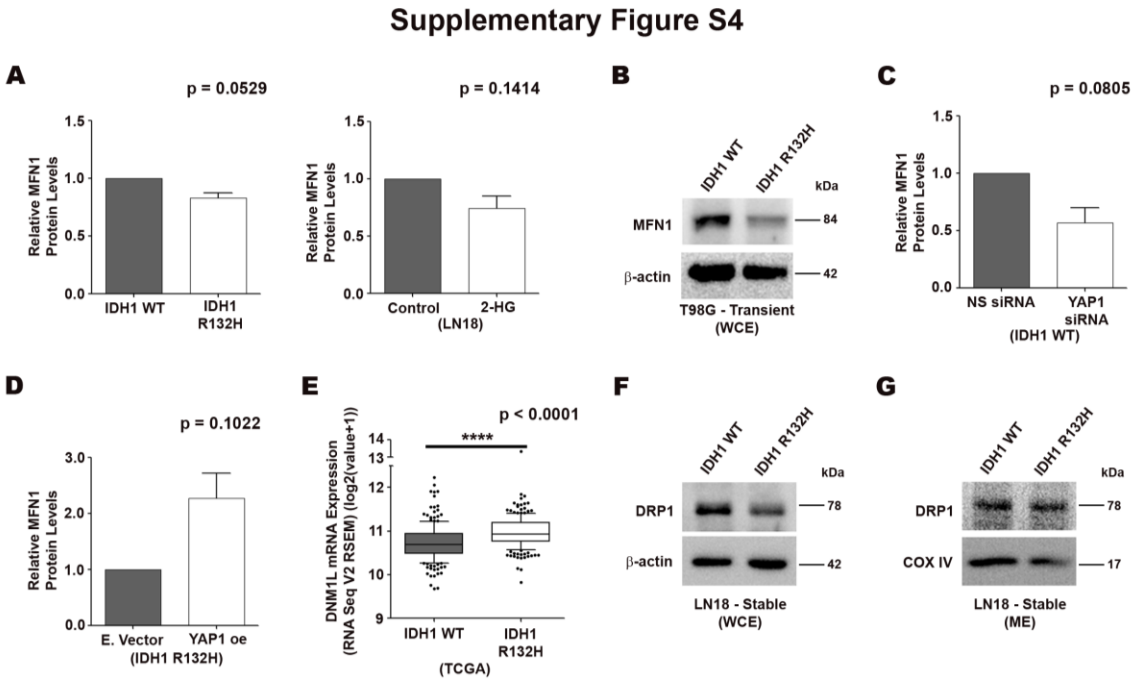

Fig. S4. Altered MFN1 and DRP1 levels in IDH1 R132H cells

A. Densitometric analysis shows lower MFN1 protein levels in IDH1 R132H cells and 2-HG-treated LN18 cells

B. Immunoblot shows a decrease in MFN1 levels in T98G cells transiently transfected with IDH1 R132H. The blots are representative of two independent experiments with similar results. WCE, whole cell extract

C. Densitometry shows a reduction in MFN1 protein levels upon siRNA-mediated knockdown of YAP1 in IDH1 WT cells

D. Densitometry shows an increase in MFN1 levels on overexpressing YAP1 in IDH1 R132H cells

E. TCGA data analysis shows higher DNM1L (DRP1) expression in IDH1 R132H gliomas as compared to IDH1 WT gliomas. Data from N=204 IDH1 WT and 206 IDH1 R132H patients from TCGA have been used for analysis. Whiskers represent 10-90 percentile. ****, p<0.0001 (Two-tailed student's t-test)

F. Immunoblots show reduced levels of DRP1 in IDH1 R132H cells. The blots are representative of three independent experiments with similar results.

G. Immunoblots with mitochondrial protein fractions show higher recruitment of DRP1 in the mitochondria of IDH1 R132H cells as compared to IDH1 WT. The blots are representative of two independent experiments with similar results.

All densitometry graphs represent data expressed as fold change over respective controls, presented as mean ± SEM. N=3 biological replicates. Paired two-tailed student's t-test was used for statistical analysis. WCE, whole cell extract; ME, mitochondrial extract; NS siRNA, Non-specific siRNA; E. vector, Empty vector; YAP1 oe, YAP1 overexpression

Supplementary Figure S5

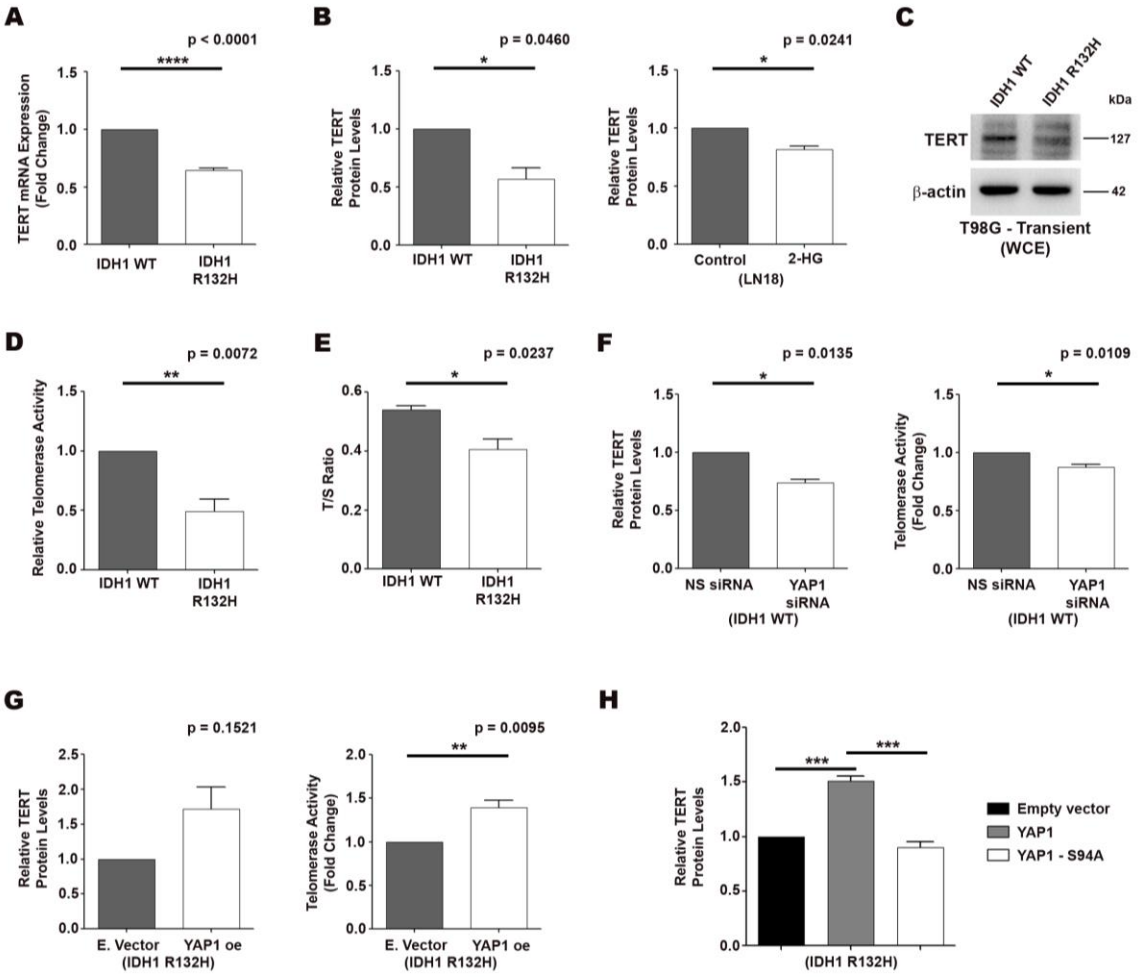

Fig. S5. YAP1-dependent TERT expression and telomerase activity

A. qRT-PCR shows reduced TERT mRNA levels in IDH1 R132H cells. Data are expressed as fold change over IDH1 WT and presented as mean ± SEM. N=5 biological replicates. ****, $p<0.0001$ (Two-tailed student's t-test)

B. Densitometric analysis of immunoblots shows lower TERT protein levels in IDH1 R132H cells and 2-HG-treated LN18 cells as compared to IDH1 WT and control cells respectively

C. Immunoblots show a decrease in TERT levels in T98G cells transiently transfected with IDH1 R132H. The blots are representative of two independent experiments with similar results. WCE, whole cell extract

D. Telomeric repeat amplification protocol (TRAP) assay shows decreased telomerase activity in IDH1 R132H cells as compared to IDH1 WT. Data are expressed as fold change over IDH1 WT and presented as mean ± SEM. N=3 biological replicates. **, $p<0.01$ (Two-tailed student's t-test)

E. Telomere length measurement by qPCR shows a reduction in IDH1 R132H cells. Data are presented as mean ± SEM. N=3 biological replicates. T/S ratio, ratio of telomere to single copy gene 36B4; *, $p<0.05$ (Two-tailed student's t-test)

F. Densitometry shows a reduction in TERT protein levels upon siRNA-mediated knockdown of YAP1 in IDH1 WT cells. TRAP assay reveals a decrease in telomerase activity on siRNA-mediated knockdown of YAP1 in IDH1 WT cells

G. Densitometry shows an increase in TERT protein levels upon overexpression of YAP1 in IDH1 R132H cells. TRAP assay reveals an increase in telomerase activity on overexpressing YAP1 in IDH1 R132H cells

H. Densitometric analysis shows an increase in TERT levels on overexpressing wild type YAP1 in IDH1 R132H cells, but not on overexpressing YAP1-S94A mutant

All densitometry graphs represent data expressed as fold change over respective controls, presented as mean ± SEM. N=3 biological replicates. *, $p<0.05$; **, $p<0.01$; ***, $p<0.001$. Comparisons between two groups were done using paired two-tailed student's t-test, and comparisons among multiple groups were done using one-way ANOVA with Tukey's multiple comparison test. NS siRNA, Non-specific siRNA; E. vector, Empty vector; YAP1 oe, YAP1 overexpression

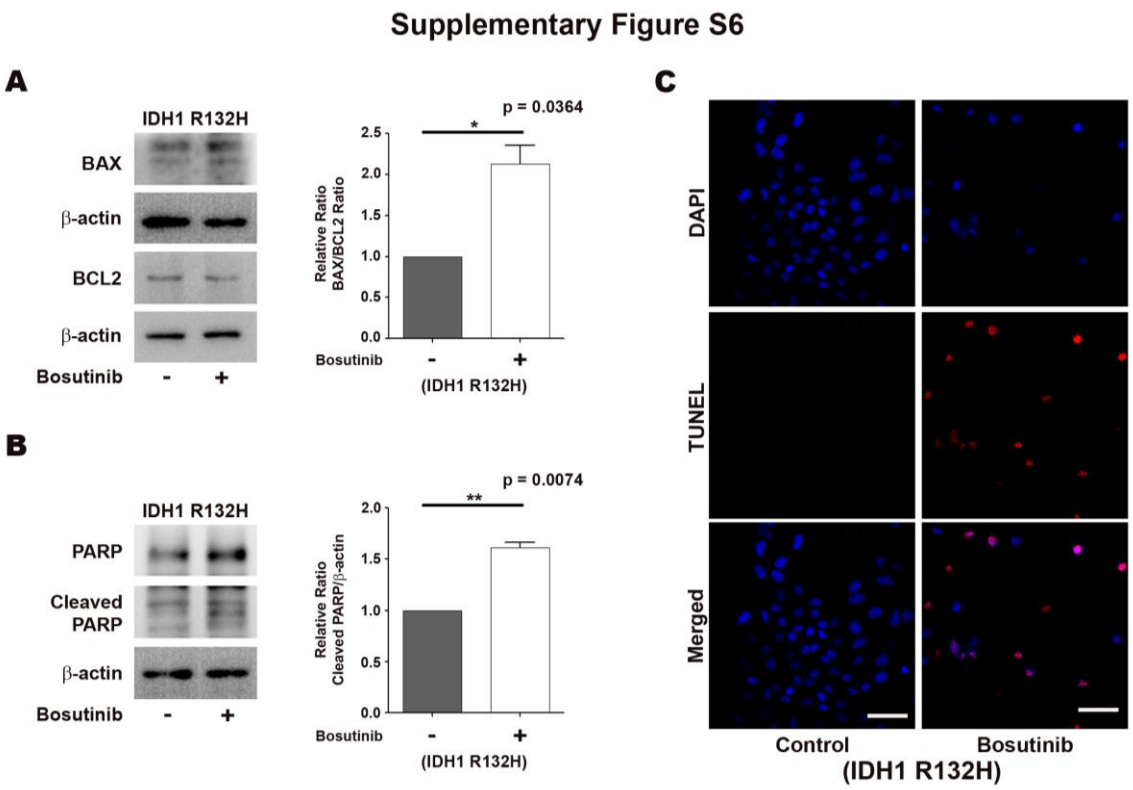

Fig. S6. Apoptosis in IDH1 R132H cells upon Bosutinib treatment

A. Immunoblots and densitometric analysis show an increase in BAX/BCL2 ratio in Bosutinib-treated IDH1 R132H cells

B. Immunoblots and densitometric analysis show an increase in cleaved PARP levels in Bosutinib-treated IDH1 R132H cells

C. Maximum intensity projections of confocal microscopic images of IDH1 R132H cells showing TUNEL staining under control and Bosutinib-treated conditions

Graphs represent data expressed as fold change over control, presented as mean ± SEM. N=3 biological replicates. *, $p<0.05$; **, $p<0.01$ (Paired two-tailed student's t-test)

Supplementary Figure S7

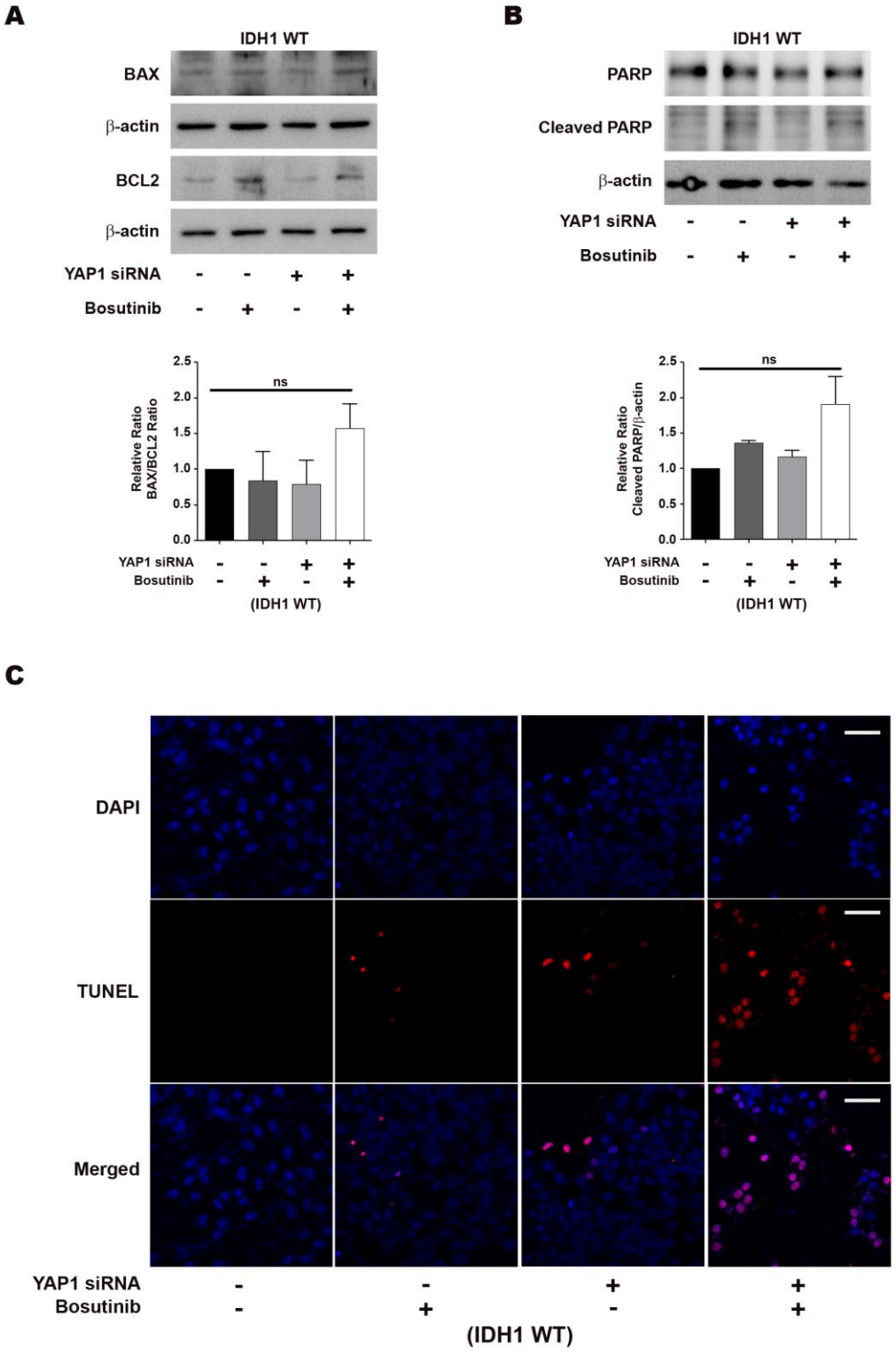

Fig. S7. Apoptosis in IDH1 WT cells upon YAP1 depletion and Bosutinib treatment

A. Immunoblots and densitometric analysis show an increase in BAX/BCL2 ratio upon Bosutinib treatment along with siRNA-mediated knockdown of YAP1 in IDH1 WT cells
B. Immunoblots and densitometric analysis show an increase in cleaved PARP levels in IDH1 WT cells on treatment with Bosutinib along with siRNA-mediated knockdown of YAP1.
C. Maximum intensity projections of confocal microscopic images of IDH1 WT cells showing TUNEL staining under the specified conditions

Graphs represent data expressed as fold change over control, presented as mean ± SEM. N=3 biological replicates (N=2 for cleaved PARP). ns, not significant (One-way ANOVA with Tukey's multiple comparison test)